NOTICE

The quality of this microform is heavily dependent upon the quality of the original thesis submitted for microfilming. Every effort has been made to ensure the highest quality of reproduction possible.

If pages are missing, contact the university which granted the degree.

Some pages may have indistinct print especially if the original pages were typed with a poor typewriter ribbon or if the university sent us an inferior photocopy.

Reproduction in full or in part of this microform is governed by the Canadian Copyright Act, R.S.C. 1970, c. C-30, and subsequent amendments.

AVIS

La qualité de cette microforme dépend grandement de la qualité de la thèse soumise au microfilmage. Nous avons tout fait pour assurer une qualité supérieure de reproduction.

S'il manque des pages, veuillez communiquer avec l'université qui a conféré le grade.

La qualité d'impression de certaines pages peut laisser à désirer, surtout si les pages originales ont été dactylographiées à l'aide d'un ruban usé ou si l'université nous a fait parvenir une photocopie de qualité inférieure.

La reproduction, même partielle, de cette microforme est soumise à la Loi canadienne sur le droit d'auteur, SRC 1970, c. C-30, et ses amendements subséquents.

Canada

ISBN 0-315-53841-4

Radiation from Microstrip Transmission Lines

by

John P. Simpson

A Thesis submitted to the
School of Graduate Studies and Research
in partial fulfillment of the requirements
for the degree of

Master of Applied Science

Ottawa-Carleton Institute for
Electrical Engineering

Department of Electrical Engineering
Faculty of Engineering
University of Ottawa

November, 1987

I hereby declare that I am the sole author of this document. I authorize the University of Ottawa to lend this document to other individuals or institutions for the purpose of scholarly research.

I further authorize the University of Ottawa to reproduce this document by photocopying or by other means, in total or in part, at the request of other institutions or individuals for the purpose of scholarly research.

ACKNOWLEDGMENTS

The author wishes to convey his deepest gratitude to Dr. G. Costache for his help and encouragement during the course of this work.

The author would also like to thank Mr. R.R. Goulette of Bell Northern Research with whom many discussions on this topic have taken place.

Finally I would like to thank my wife for her understanding and patience during this endeavor.

ABSTRACT

Analysis using numerical and analytical methods is used to determine the electric field radiated from a microstrip transmission line of the type used in printed circuit board technologies. The techniques used establish a means of determining the status of a particular design with respect to regulatory emissions requirements imposed on digital electronic devices. Analysis and experimental measurements are compared for a sample microstripline operating at 100 MHz. The measurements are performed at an 'Open Field' test site of the type specified by the Federal Communications Commission in the U.S.A. for verification of compliance to their regulations

Table of Contents

1 INTRODUCTION 1
1.1 Approach 3

2 THEORY 7
2.1 Approach 7
2.2 Electric Field from the Vector Magnetic Potential .. 8
2.3 Pocklington's Equation 11
2.4 Finite Element Theory 13
2.4.1 Microstrip Capacitance 21
2.4.2 Moment Method 24

3 Analysis 27
3.1 Structure to be analyzed 29
3.2 Characteristic Impedance 32
3.3 Multiple Images 36
3.4 Electric Field Calculations 40
3.4.1 Method I 40
3.4.2 Method II 45
3.5 Test Site Calculations 46
3.6 Discussion of Calculated Results 51

4 Experimental Measurements 54
4.1 Characteristic Impedance 54
4.2 Radiated fields 56
4.2.1 Measurement setup 56
4.3 Test method 59
4.4 Test Results 60

5 Conclusions 63

6 Appendix 65

7 References 70

Table of Figures

1 Cross sectional view of a microstripline 4
2 Coordinate orientation 10
3 Subregions 14
4 Microstrip structure 30
5 Connector and termination details 31
6 Finite Element representation 33
7 Characteristic impedance 35
8 Multiple image presentation 37
9 Orientation of transmission line 43
10 Test orientation 47
11 Ez vs height for various termination impedances 49
12 Ex vs height for various termination impedances 50
13 Microstrip input impedance 55
14 Photograph of test setup 58
15 Comparison of calculated and measured results 61
16 Comparison of calculated and measured results 62

Table of Tables

I Calculated characteristic impedance 34
II Calculated array factors 39
III Radiated fields results - Method I 44
IV Radiate fields results - Method II 45

1 INTRODUCTION

During the past few years the emphasis on digital electronics has been to increase the operational speed of circuits, resulting in logic devices becoming faster and capable of higher drive levels. To accommodate the higher speeds, microstrip and stripline transmission lines have been employed to interconnect the high speed circuits. The benefit of these techniques are controlled impedance structures which would minimize signal reflections and reduce waveshape distortion. Unfortunately with the increase in speed and drive levels comes an increase in electromagnetic radiation from these transmission lines. Problems in the form of Electromagnetic Interference resulting from the digital circuits prompted the Federal Communications Commission (FCC) in the U.S.A. [1] and other similar agencies throughout the world to adopt regulations limiting the levels of Radiated Emissions from digital electronic devices.

The introduction of these regulations has resulted in yet another dimension to the design process. Not only does the design engineer have to be concerned with meeting functional, aesthetic, reliability and safety issues, he must now address Electromagnetic Compatibility (EMC) requirements.

Concern over EMC has been commonplace in the military and aerospace industries for many years. The design cycles in these industries include component, sub-system, and prototype system tests and re-design to ensure sound electromagnetic compatibility in the design.

In contrast, to capture a commercial market, the demand for short design cycles usually precludes the various sub-system tests and re-design stages present in a military program. A weak EMC design may not be detected until final compliance testing begins. At that point the options for corrective action may be

limited. Heavy containment (shielding, filtering etc.) would be the quickest solution but would be costly and may detract from the aesthetic appeal of the product. Alternatively the product introduction could be delayed while a re-design takes place. Unfortunately delays to a product introduction may seriously affect the product's success in a fast-paced market.

To minimize these risks, analysis with respect to the electromagnetic emissions and susceptibility of a design early in the product development cycle should be a standard requirement of any development process. Weaknesses highlighted early in the design stages can be corrected when the range of options open to the design engineer is much greater. Perhaps shielding is still required, at least the packaging designers can include it in their design without seriously affecting the product appearance. Alternatively, a design may have been too conservative in applying EMC controls. Costs could be avoided early rather than in a cost reduction cycle after the product has been compliance tested and introduced to the market place.

The consequence of not attempting to predict the emission levels during the design stage of product development is potentially costly re-design of the printed circuit board and/or the equipment package. In addition, costly packaging options may be avoided by addressing the circuit board performance and taking corrective action at that level.

1.1 Approach

Several approaches have previously been presented to predict emissions from transmission lines and printed circuit boards [2,3,4]. Generally these assume an ideal transmission line, establish the current distribution on the line for a given source and load impedance and then calculate the resultant electric field in free space.

FCC however require the product in question be tested not in free space but over a conducting ground plane where the measured field is the sum of the direct and ground reflected fields. The vector sum of these fields is dependent upon the test configuration, radiation pattern of the equipment under test and the receiving antenna and the frequency of the radiation being tested. Although ground conductivity would also affect the measurements, the various regulations require a metallic ground plane (or sufficiently high ground conductivity) that the variability due to the ground is minimum.

The work presented here will be to calculate the radiated electric field from a typical microstrip transmission line based on the the FCC test requirements and compare the results with measurements of the microstrip at an FCC type open field test facility.

Also to be investigated in this work is the influence of the dielectric on the radiated emissions. The presence of the dielectric will definitely determine the characteristic impedance of the microstrip transmission line. In addition multiple images resulting from the air/dielectric boundary could have an influence on the radiated fields and will thus be considered.

The general configuration of a microstrip structure used in digital printed circuit board design is illustrated in Figure 1 below

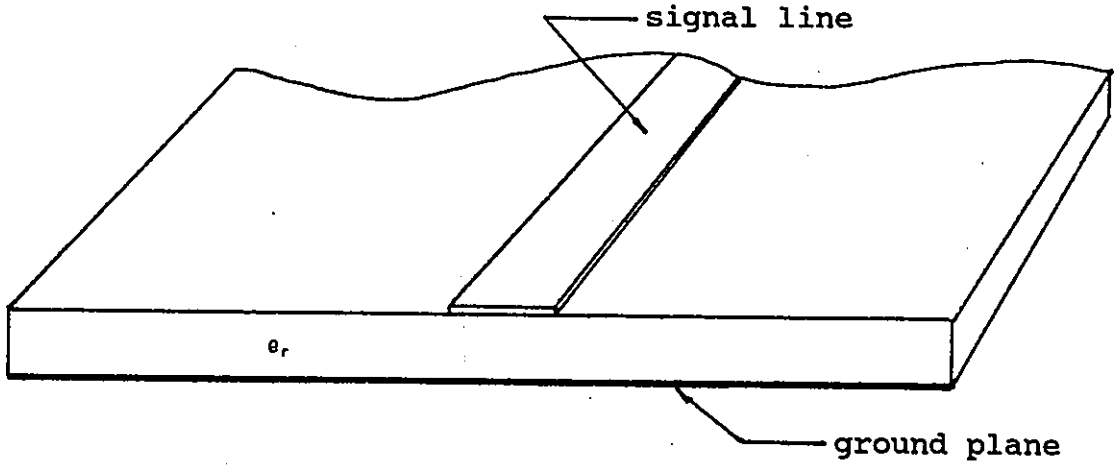

Figure 1
Cross sectional view of a microstrip transmission line

The materials used to construct a printed circuit board for digital applications in the commercial market are G-10 or FR-4 glass epoxy dielectrics ($\epsilon_r = 4.5$) with 1 ounce (.0017" thick) copper cladding.

The thickness of the dielectric generally varies depending upon the application. Double sided circuit boards (copper cladding on both sides) range from .032"-.063" thick whereas multi-layer (buried conductor layers within the dielectric) printed circuit boards may have dielectric layers between conductors as thin as .01".

At microwave frequencies it is common practice to construct a stripline structure (signal line located between two ground planes). For densely packed digital printed circuit boards it is extremely costly to produce a board where many connections must be made to a buried signal layer. To simplify construction and reduce costs, the general method is to place the signal lines on the outer surfaces and laminate the power and ground planes in the dielectric.

It is shown that the electric field intensity produced by such a structure is proportional to the separation distance between the conductor and the associated ground return. Also, for the range of dielectric thicknesses found between double layer and multi-layer circuit boards, the dielectric thickness to conductor width ratio does not vary significantly for a given characteristic impedance.

As a result of these conditions and the added complexity of constructing a multi-layer printed circuit board, this work will focus on the investigation of a microstrip based upon the double sided construction technique.

Calculations of the electric field are done analytically using the magnetic vector potential and numerically using the Method of Moments technique for comparative purposes. Both techniques have associated strengths and weaknesses which may be of interest in this application.

The intent is to use a frequency in the range known to cause problems with FCC compliance of digital products. The frequency range for FCC radiated emissions is 30-1000 MHz., although most designs result in the majority of the energy being radiated in the 30-130 MHz range. For this reason the frequency selected for this work is 100 MHz.

2 THEORY

In the study of electromagnetic phenomena, problems generally fall into two distinct categories, namely analysis and synthesis. In analysis type problems the source and boundary conditions are generally known and the objective is to determine the fields resulting from the source. By contrast, a synthesis problem usually begins with a desired radiated field and the source and boundary conditions must be found to produce such a field. Since the main concern in this work is to determine the electromagnetic fields produced by a microstrip structure the problem is one of analysis. The microstrip structure and source conditions (currents) are defined based on a need to transmit information along the transmission line. These parameters are chosen to permit efficient and reliable transmission, generally without regard for the radiation produced. The object of this work is to analyze the radiated fields for such a transmission line.

2.1 Approach

Two methods will be considered for the analysis presented in this work. The first method will be an analytical approach based on calculation of the electric field from the magnetic vector potential. The characteristic impedance of the microstrip will be determined using the Finite Element Method and compared with a closed form approximation. Once the characteristic impedance is known, the current distribution along the line can be determined for a given source and load condition and the current used in the magnetic vector potential calculations.

The second method will be to solve Pocklington's equation numerically using the Method of Moments for comparative purposes.

2.2 Electric Field from the Vector Magnetic Potential

Appendix I presents the derivation of the magnetic vector potential which although not a physical entity, is the first step to determining the electric field resulting from an electric current.

Consider the expression [5]:

$$\bar{E} = \bar{E}_A + \bar{E}_F = -j\omega\bar{A} - \frac{j}{\omega\mu\epsilon}\nabla(\nabla\cdot\bar{A}) - \frac{1}{\epsilon}\nabla\times F \tag{1}$$

where $\bar{A}$ is the magnetic vector potential and F represents the vector electric potential given by:

$$\bar{A} = \frac{\mu}{4\pi}\int\int_{v'}\int J\frac{e^{-jkR}}{R}dv' \tag{2}$$

$$F = \frac{\epsilon}{4\pi}\int\int_{v'}\int \bar{M}\frac{e^{-jkR}}{R}dv' \tag{3}$$

where $k = 2\pi/\lambda$

The sources in the above formulas are J, the electric current density and $\bar{M}$, the magnetic current density.

Since the transmission line contains an electric current source only ($\bar{M} = 0$) then the contribution due to the vector electric potential vanishes:

$$\bar{E}_F = -\frac{1}{\epsilon}\nabla\times F = 0 \tag{4}$$

From Figure 2, J is a line source in the z direction and equation (2) reduces to:

$$A = \frac{\mu}{4\pi}\int_0^l I_o(z')\frac{e^{-jkR}}{R}dz' \tag{5}$$

Substituting (5) back into (1) now results, for far field situations which are of interest to FCC, in [1]:

$$E = -j\omega A \tag{6}$$

The current $I(z')$ along the transmission line can be determined providing the source and load conditions along with the characteristic impedance (Zo) are known.

The characteristic impedance can be found by a number of methods including the Method of Moments and the Finite Element Method or using a closed form expression as given in appendix II. The approach used in this work will be that of Finite Elements [6] and the results compared with those obtained by using the analytical technique presented in appendix II.

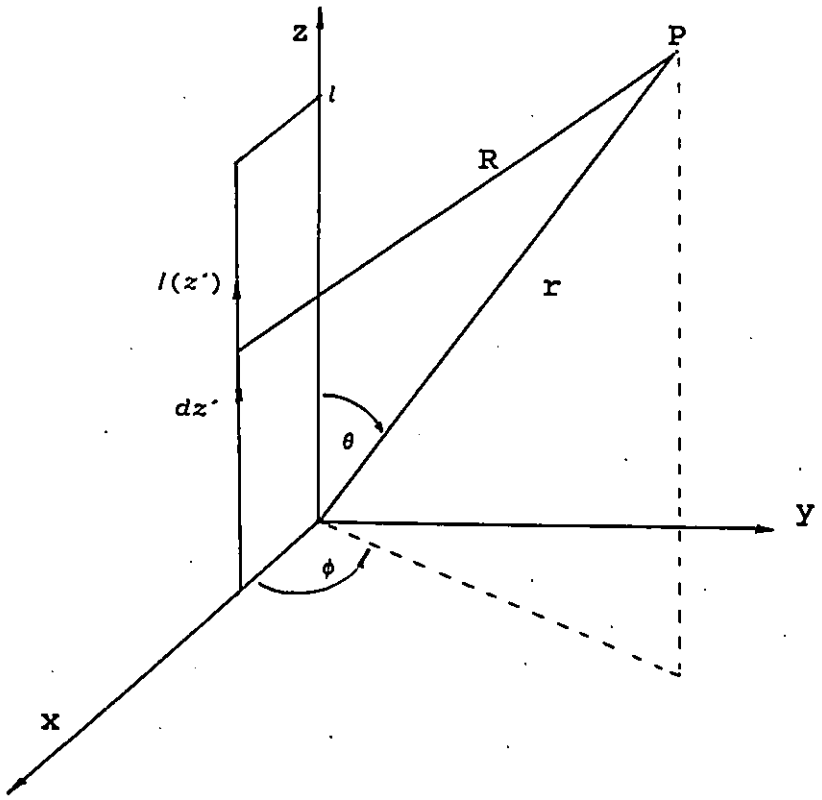

Fig. 2

Coordinate system for transmission line

2.3 Pocklington's Equation

The Method of Moments technique used to determine the electric field produced by a current source is a numerical technique which is used to solve an integral equation. Two popular equations which are used in this application are Hallen's and Pocklington's integral equations. Pocklington's equation, which is more general, will be used here.

Returning to equation (1) and considering the case where only electric currents exists:

$$\bar{E} = \bar{E}_A + \bar{E}_F = -j\omega\bar{A} - \frac{j}{\omega\mu\epsilon}\nabla(\nabla\cdot\bar{A}) \tag{7}$$

Assuming z direction current flow only as shown in Figure 2, then the magnetic vector potential has only a z component ($\bar{A} = \hat{a}_z A_z$) and the electric field expression can be written as:

$$E_z = -j\omega A_z - \frac{j}{\omega\mu\epsilon}\frac{\partial^2 A_z}{\partial z^2} \tag{8}$$

This formula can be re-arranged and after a few manipulations the relationship between the magnetic vector potential and the electric field is obtained:

$$\frac{\partial^2 A_z}{\partial z^2} + \omega^2\mu\epsilon A_z = j\omega\mu\epsilon E_z \tag{9}$$

At this point the magnetic vector potential can be expressed in terms of the current density according to (5) and an integral equation in terms of current density is obtained [5]:

$$\int\int\int J_z(x',y',z')\left(\frac{\partial^2}{\partial z^2}+k^2\right)\frac{e^{-jkR}}{4\pi R}dv' = j\omega\mu\epsilon E_z \qquad (10)$$

where:

$$k = \omega^2\mu\epsilon$$

$$R = \sqrt{(x-x')^2+(y-y')^2+(z-z')^2}$$

Although figure 2 presents a line current in the z direction, in reality a wire of finite diameter would be present.

Assuming the wire to be of infinite conductivity with the current density J_z confined to the surface of the wire and uniform about the circumference of the wire, then an equivalent current I_z can be located on the axis of the wire. Equation (10) can then be simplified to:

$$\int_{-l/2}^{l/2} I_z(z')\left[\left(\frac{\partial^2}{\partial z^2}+k^2\right)\frac{e^{-jkR}}{4\pi R}\right]dz' = j\omega\epsilon E_z^s(z) \qquad (11)$$

where E_z^s represents the scattered free-space field.

2.4 Finite Element Theory

As outlined in Section 2.2, the current distribution along the transmission line must be known. Closed form expressions exist for this purpose [7,8,9] but are of limited applicability. Generally they are confined to specific track width to dielectric thickness ratios to maintain reasonable accuracy. To circumvent this problem numerical techniques such as the Finite Element Method can be used to determine the capacitance per unit length of the transmission line which will then be used to determine the characteristic impedance.

In determining the characteristic impedance of the microstrip, the assumption will be made that it is supporting a TEM mode of propagation. Although not absolutely correct, it is sufficient for most microstripline problems [7].

The objective here is to determine the capacitance per unit length of the line which can be determined from the energy stored in the electric field. The Finite Element Method is used to determine the field distribution and hence the energy per unit length for the microstrip.

The electrostatic potential in free space (ϕ) will obey Poisson's Equation given by:

$$\nabla^2 \phi = f \tag{12}$$

where the source term is the ratio between the charge density and the permittivity.

$$f = -\rho/\epsilon$$

A functional $F(\phi)$ relating to the energy in the region D is defined as:

$$F(\phi)=\int_D(\nabla\phi)^2dxdy-2\int_D\phi f dxdy \tag{13}$$

The potential ϕ will be distributed within the region D so as to minimize the potential energy and thus the functional $F(\phi)$.

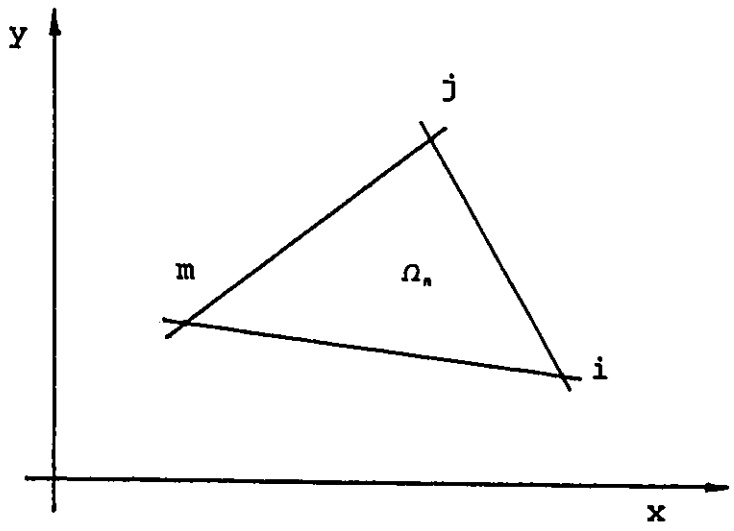

Figure 3 - Subregions

Dividing the region D into N subregions Ω_n such as shown in Figure 3 the functional now becomes:

$$F(\phi)=\sum_{1}^{N}\int_{\Omega_n}(\nabla\phi)^2dxdy-2\sum_{1}^{N}\int_{\Omega_n}\phi f dxdy \tag{14}$$

Let the potential in each triangle be a linear trial function given as:

$$\phi(x,y)=C_0+C_1x+C_2y \tag{15}$$

The potential at each vertex of a given triangle will then be given by:

$$\begin{pmatrix}\phi_i\\ \phi_j\\ \phi_m\end{pmatrix}=\begin{pmatrix}1 & x_i & y_i\\ 1 & x_j & y_j\\ 1 & x_m & y_m\end{pmatrix}\begin{pmatrix}C_0\\ C_1\\ C_2\end{pmatrix} \tag{16}$$

where each ϕ_i,ϕ_j,ϕ_m must satisfy the continuity between adjacent triangles. The variational parameters C_0,C_1 and C_2 can now be replaced with new variational parameters, the node potentials ϕ_i,ϕ_j and ϕ_m by solving equation (16) for C_0,C_1 and C_2.

The variational parameters can now be written as:

$$C_0 = [\phi_i(x_i y_m - x_m y_i) + \phi_j(x_m y_i - x_i y_m) + \phi_m(x_i y_j - x_j y_i)]/2A \qquad (17)$$

$$C_1 = [\phi_i(y_i - y_m) + \phi_j(y_m - y_i) + \phi_m(y_i - y_j)]/2A \qquad (18)$$

$$C_2 = [\phi_j(x_m - x_i) + \phi_j(x_i - x_m) + \phi_m(x_j - x_i)]/2A \qquad (19)$$

where:

$$2A = \begin{vmatrix} 1 & x_i & y_i \\ 1 & x_j & y_j \\ 1 & x_m & y_m \end{vmatrix}$$

is the area of the triangle.

Substituting for C_0, C_1 and C_2 into (15), the potential in each triangle can be written as:

$$\phi(x,y) = \alpha_i(x,y)\phi_i + \alpha_j(x,y)\phi_j + \alpha_m(x,y)\phi_m \qquad (20)$$

where:

$$\alpha_i = [(x_j y_m - x_m y_j) + (y_j - y_m)x + (x_m - x_j)y]/2A \qquad (21)$$

$$\alpha_j = [(x_m y_i - x_i y_m) + (y_m - y_i)x + (x_i - x_m)y]/2A \qquad (22)$$

$$\alpha_m = [(x_i y_j - x_j y_i) + (y_i - y_j)x + (x_j - x_i)y]/2A \qquad (23)$$

The minimizing condition for the functional $F(\phi)$ describing the potential distribution can be written as:

$$\frac{\partial F(\phi_i)}{\partial \underline{\phi}_i} = 0 \qquad (i = 1,2 \ldots N) \tag{24}$$

where:

$$\frac{\partial F}{\partial \underline{\phi}} = \begin{pmatrix} \frac{\partial F}{\partial \phi_1} \\ \cdot \\ \cdot \\ \cdot \\ \frac{\partial F}{\partial \phi_N} \end{pmatrix} \tag{25}$$

which in a matrix form is described by a system of algebraic equations given by:

$$S\underline{\phi} = \underline{b} \tag{26}$$

The contribution for each triangle in the final system of equations is now evaluated.

Returning to (14) one can write the functional expression as a superposition of integrals given by:

$$F(\phi)=\sum_{1}^{N}\int_{\Omega_n}(\nabla\phi)^2dxdy-2\sum_{1}^{N}\int_{\Omega_n}\phi f\,dxdy \tag{27}$$

The triangle described by nodes i,j and m brings a contribution to the functional evaluated by:

$$F_k=\int_{\Omega_k}(\nabla\phi)^2dxdy-\int_{\Omega_k}\phi f\,dxdy \tag{28}$$

where the trial function is a linear interpolation between unknown potentials of the nodes, $\phi=\alpha_i(x,y)\phi_i+\alpha_j(x,y)\phi_j+\alpha_m(x,y)\phi_m$

The gradient of the potential required to evaluate the above integrals can now be written as:

$$\nabla\phi=\left(i\frac{\partial}{\partial x}+j\frac{\partial}{\partial y}\right)\left(\alpha_i(x,y)\phi_i+\alpha_j(x,y)\phi_j+\alpha_m(x,y)\phi_m\right)$$

$$=\left(\hat{i}\frac{\partial\alpha_i}{\partial x}+\hat{j}\frac{\partial\alpha i}{\partial y}\right)\phi_i+\left(\hat{i}\frac{\partial\alpha_j}{\partial x}+\hat{j}\frac{\partial\alpha j}{\partial y}\right)\phi_j+\left(\hat{i}\frac{\partial\alpha_m}{\partial x}+\hat{j}\frac{\partial\alpha_m}{\partial y}\right)\phi_m$$

$$=\{[(y_j-y_m)\hat{i}+(x_m-x_j)\hat{j}]\phi_i+[(y_m-y_i)\hat{i}+(x_i-x_m)\hat{j}]\phi_j+$$
$$+[(y_i-y_j)\hat{i}+(x_j-x_i)\hat{j}]\phi_m\}/2A \tag{29}$$

The derivative of the functional with respect to the node potentials

$$\frac{\partial F_k}{\partial \phi_i}, \frac{\partial F_k}{\partial \phi_k} \quad \& \quad \frac{\partial F_k}{\partial \phi_m} \tag{30}$$

are now determined:

$$\begin{aligned}\frac{\partial F_k}{\partial \phi_i} = \{&\left[(y_j - y_m)^2 + (x_j - x_m)^2\right]\phi_i \\ &-\left[(y_i - y_m)(y_j - y_m) + (x_i - x_m)(x_j - x_m)\right]\phi_j \\ &-\left[(y_i - y_j)(y_m - y_i) + (x_i - x_j)(x_m - x_j)\right]\phi_m\}/2A \\ &= \left(S_{ii}\phi_i + S_{ij}\phi_j + S_{im}\phi_m\right)/2A\end{aligned} \tag{31}$$

$$\begin{aligned}\frac{\partial F_k}{\partial \phi_j} = \{&-\left[y_j - y_m)(y_i - y_m) + (x_j - x_m)(x_i - x_m)\right]\phi_i \\ &+\left[(y_m - y_i)^2 + (x_i - x_m)^2\right]\phi_j \\ &-\left[(y_j - y_i)(y_m - y_i) + (x_j - x_i)(x_m - x_i)\right]\phi_m\}/2A \\ &= \left(S_{ji}\phi_i + S_{jj}\phi_j + S_{jm}\phi_m\right)/2A\end{aligned} \tag{32}$$

$$\begin{aligned}\frac{\partial F_k}{\partial \phi_m} = \{&-\left[(y_m - y_i)(y_j - y_i) + (x_m - x_i)(x_j - x_i)\right]\phi_i \\ &-\left[(y_m - y_j)(y_j - y_i) + (x_m - x_i)(x_j - x_i)\right]\phi_j \\ &+\left[(y_i - y_j)^2 + (x_j - x_i)^2\right]\phi_m\}/2A \\ &= \left(S_{mi}.\phi_i + S_{mj}\phi_j + S_{mm}\phi_m\right)/2A\end{aligned} \tag{33}$$

From equations (31,32 and 33), one can see that the contributions from each triangle denoted by the S terms can be easily calculated from the node coordinates. The calculations are then performed for each triangle and the results substituted back into the system of equations.

Returning to equation (26), it can now be seen the triangle with vertices i,j,m contributes to the final matrix as follows:

$$\begin{pmatrix} S_{11} & S_{12} & \cdot & \cdot & \cdot & \cdot & \cdot \\ S_{21} & \cdot & \cdot & \cdot & \cdot & \cdot & \cdot \\ \cdot & \cdot & S_{ii} & S_{ij} & S_{im} & \cdot & \cdot \\ \cdot & \cdot & S_{ji} & S_{jj} & S_{jm} & \cdot & \cdot \\ \cdot & \cdot & S_{mi} & S_{mj} & S_{mm} & \cdot & \cdot \\ \cdot & \cdot & \cdot & \cdot & \cdot & \cdot & \cdot \end{pmatrix} \begin{pmatrix} \phi_1 \\ \cdot \\ \phi_i \\ \phi_j \\ \phi_m \\ \cdot \end{pmatrix} = \begin{pmatrix} b_1 \\ \cdot \\ b_i \\ b_j \\ b_m \\ \cdot \end{pmatrix}$$

The $b_i, b_j,$ and b_m terms in (34) are similarly derived from $\int_\Omega f\phi dxdy$.

The triangles with nodes located on the Dirichlet boundaries will bring contributions to the final system of equations as follows. The contribution from the Dirichlet node is reflected into the right hand side of the final system of equations while the contribution from the free nodes will appear in the system matrix.

2.4.1 Microstrip Capacitance

To determine the characteristic impedance of the microstrip structure, the capacitance per unit length of the structure is required.

The electric field needed for the calculations can be expressed in terms of the scalar potential as:

$$\bar{E} = -\nabla\phi \tag{35}$$

In Section 2.4 the potential function for each triangle was given by equation (15). Substituting this equation into (35), the electric field in each triangle will now be given by:

$$\bar{E} = -\left[\hat{i}\frac{\partial\phi}{\partial x} + \hat{j}\frac{\partial\phi}{\partial y}\right] \tag{36}$$

$$= -\hat{i}C_1 - \hat{j}C_2$$

The electric field in each triangle can now be calculated from C_1 and C_2 (equations (18) & (19)).

Once the electric field $\bar{E}(x,y)$ has been determined, the potential per unit length can be calculated from [10]:

$$U = \frac{1}{2}\int_D \epsilon E^2 d\tau = \frac{1}{2}\int_D\int \epsilon E^2 dx dy \tag{37}$$

On the other hand the work required to charge a capacitor is given by the expression:

$$W = \int_0^Q \frac{q}{c} dq = \frac{Q^2}{2C} \tag{38}$$

and Q , the total charge on the capacitor is given by

$$Q = CV \tag{39}$$

where:

C = capacitance

V = voltage

The work required to charge the capacitance of the microstripline is now given by:

$$W_e = \frac{CV^2}{2} \tag{40}$$

The material used for printed circuit board applications is selected to exhibit low loss characteristics over the frequency range of use. Therefore assuming no energy is lost in charging the microstrip capacitance, all the work W_e is converted into potential energy. The capacitance of the microstrip can now be expressed in terms of the potential energy and the applied voltage:

$$C = \frac{\epsilon}{V^2} \int_D \int E^2 dx dx \tag{41}$$

The calculations are performed twice: once with $\epsilon = 1.0$ for all triangles and a second time replacing $\epsilon = 1.0$ with $\epsilon = \epsilon_r$ in all triangles located in the microstrip dielectric. The resulting capacitances can then be used to evaluate ϵ_{eff} and Z_o as follows:

$$\epsilon_{eff} = C / C_o \tag{42}$$

and

$$Z_o = \frac{1}{c\sqrt{C C_o}} \tag{43}$$

where:

C_o is the capacitance with $\epsilon = 1.0$
C is the capacitance with $\epsilon = \epsilon_r$
c the speed of light in vacuum.

2.4.2 Moment Method

The other approach mentioned in Section 2 was to use the method of moments to obtain a solution for the radiated field. Equations of the form presented in the Section 2.3 (i.e. equation (11)) are of the form:

$$L(f) = g \tag{44}$$

where: L is a linear operator
g is the source
f is the response

Since we are concerned with analysis, g is known and the objective is to determine the resulting f.

To begin, f is expanded as a linear sum [11]:

$$f(z') = c_1 f_1(z') + c_2 f_2(z') + \ldots + c_N f_N(z') = \sum_{n=1}^{N} c_n f_n(z') \tag{45}$$

The $f_n(z')$ represents a known basis or expansion function and the c_n unknown coefficients. Equation (45) can now be written as:

$$\sum_{n=1}^{N} c_n L(f_n) = g \tag{46}$$

The structure to be analyzed is then divided into N non-overlapping segments and the basis function is defined in each of these segments. Several common basis functions include constant, linear and sinusoidal forms within each segment.
A suitable inner product $\langle f, g \rangle$ can be determined and a set of weighting or testing functions (w_i) defined.

The inner product must obey the following rules:

$$\langle w, g \rangle = \langle g, w \rangle$$
$$\langle af + bg, w \rangle = a \langle f, g \rangle + b \langle g, w \rangle$$
$$\langle g^*, g \rangle > 0 \text{ if } g \neq 0$$
$$\langle g^*, g \rangle = 0 \text{ if } g = 0$$

Equation (46) now becomes:

$$\sum_{n=1}^{N} \langle w_m, Lf_n \rangle = \langle w_m, g \rangle \qquad m = 1, 2, \ldots \tag{47}$$

or writing in matrix notation

$$L_{mn} \bar{C}_n = \bar{g}_m \tag{48}$$

where:

$$L_{mn} = \begin{pmatrix} \langle w_1, Lf_1 \rangle & \cdots & \langle w_1, Lf_N \rangle \\ \vdots & & \\ \langle w_m, Lf_1 \rangle & \cdots & \langle w_m, Lf_N \rangle \end{pmatrix}$$

$$\bar{C}_n = \begin{pmatrix} c_1 \\ \vdots \\ c_N \end{pmatrix} \qquad \bar{g}_m = \begin{pmatrix} \langle w_1, g \rangle \\ \vdots \\ \langle w_m, g \rangle \end{pmatrix}$$

If the matrix L_{mn} is non-singular, then L^{-1} exists and equation (48) can be written as:

$$\bar{C} = L^{-1}\bar{g} \tag{49}$$

In choosing the expansion and weighting functions f, w one can choose Galerkin's method $(f = g)$. A requirement in defining f and w is that the f_n and w_n must be linearly independent.

Using Galerkin's method and selecting a piecewise sinusoidal expansion function has been found to be numerically efficient and highly accurate [12,13].

The approach described above has been implemented in many commercial programs. One of them, developed by J.H. Richmond [14], is used to predict the radiation from the microstrip above ground.

The intent of this work is to use the Method of Moment technique as a tool for comparative purposes and detailed theoretical expansions are beyond the scope of this work.

3 Analysis

Calculations are performed using the two previously outlined approaches with the intent to compare both calculated results with experimental measurements.

The structure to be analyzed will first be presented, followed by calculations for the array factor due to multiple images and finally the electric field calculations for both methods as follows:

Approach I (Analytical)

i. Calculate the microstrip characteristic impedance by first determining the capacitance using Finite Element techniques.

ii. Use the characteristic impedance to determine the current distribution along the length of the transmission line.

iii. Replace the microstrip structure with a parallel wire transmission line where the second wire represents the image of the microstrip conductor.

iv. Calculate the magnetic vector potential and use the result to determine the electric field.

To perform the calculations, computer programs were prepared for both the Finite Element and the electric field calculations. The programs were coded in Fortran and executed on an IBM 3033 mainframe computer.

Approach II (Numerical)

i. Replace the microstrip structure with a wire grid model. As in Approach I, the ground plane will be replaced with the conductor image below the ground.

ii. Calculate the electric field using the Method of Moments to determine the current distribution on the wire structure.

Due to the complexity of a Moment Methods program and the availability of existing programs, the program by Richmond [12] is used rather than preparing a program from scratch.

The calculations for the electric field will be performed first for the case where the transmission line is terminated in its characteristic impedance and then by introducing an unmatched case where the load impedance does not correctly match the line.

3.1 Structure to be analyzed

To produce meaningful results the aim is to reproduce as closely as possible the characteristics present for a printed circuit board used in an actual system. This implies using a board of G-10 or similar properties and configured as demonstrated in Figure 4. Details of the connector and termination mounting are presented in the photographs in Figure 5. Two resistors in parallel were used to achieve the correct matching termination resistance and to reduce the total inductance associated with the resistor leads.

This configuration will represent not only traces on a single printed circuit board but also a backplane application on which several boards may be connected. In backplane applications impedance discontinuities may be present where each board connects but the assumption here will be that the boards connecting to the back plane are impedance matched for simplicity (and good design practice !).
Since the aim is to reproduce the emissions from a digital circuit used for conventional logic (i.e. TTL) the more exotic board materials such as Diclad which are normally used for microwave frequencies will not be considered here.

Printed circuit boards generally contain traces with bends and branches which could alter their radiation pattern. Although the techniques presented here are applicable to these geometries, the intent here is to calculate the fields one would measure at an open field site. For simplicity the structure to be considered will be a straight, uniform microstrip to avoid the effects produced by any non-uniformity.

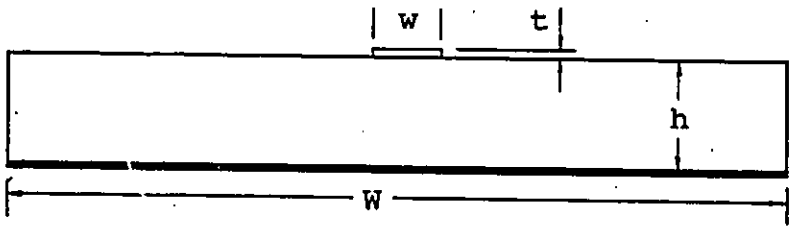

End view

w= .001m
t= 2.5e-5 m
h= .0016m
W= .2m
L= .252m

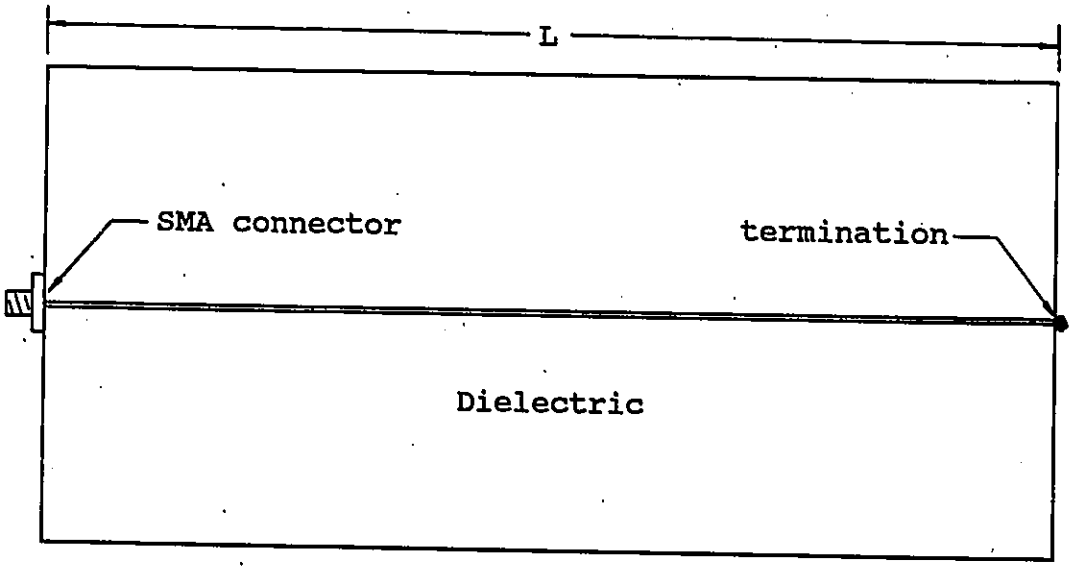

Top view

Fig. 4

Microstrip structure

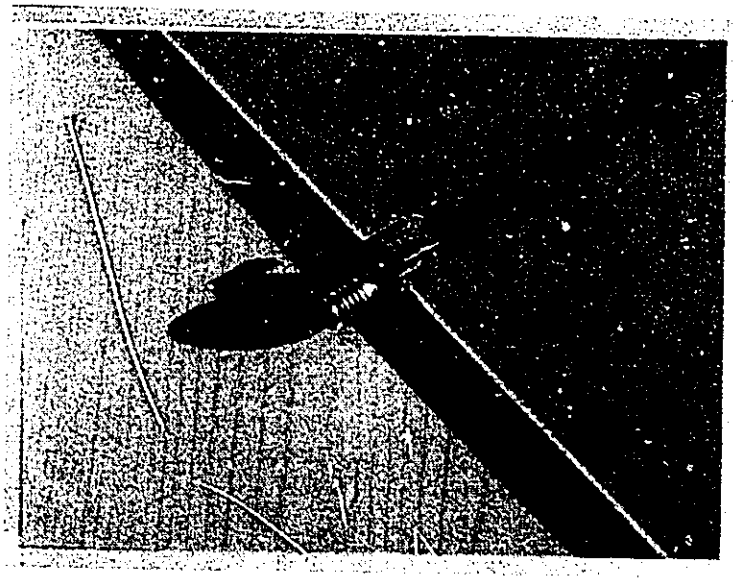

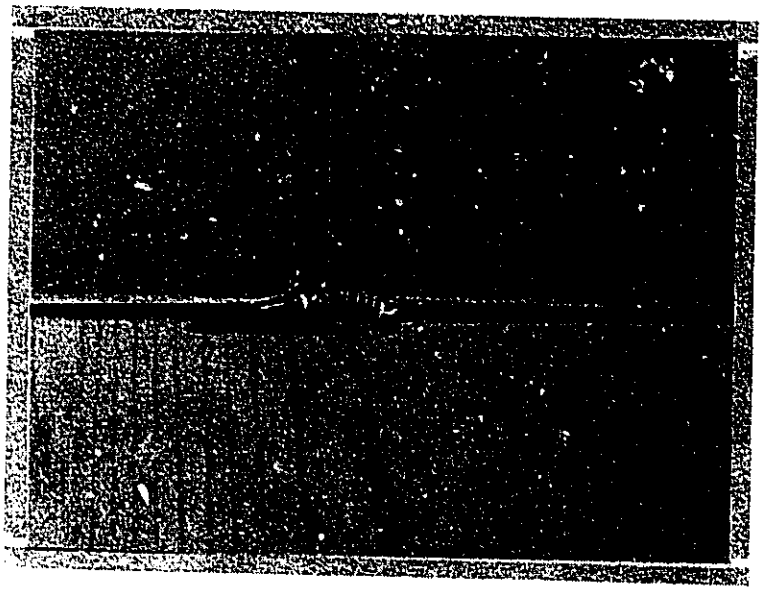

Connector and termination details

Figure 5

3.2 Characteristic Impedance

To determine the characteristic impedance for the structure presented in Figure 4, the Finite Element Method was used to determine the capacitance of the structure with and without the dielectric present. The method is only an approximation with the accuracy dependent on several factors including triangle orientation, triangle size, round off error in the computer etc.

The microstrip may be unbounded above the line, a condition not compatible with the Finite Element Method. To resolve this situation it will be assumed a cover (or adjacent printed circuit board) is located above the line and represents ground potential. Figure 6 presents the microstrip along with the assumed boundaries above and to the side of the structure. One of the triangular arrangements used for the calculations (79 triangles) is also presented. Since the structure is symmetric about the center of the line, only one half will be analyzed and the calculated energy doubled to provide for a complete system.

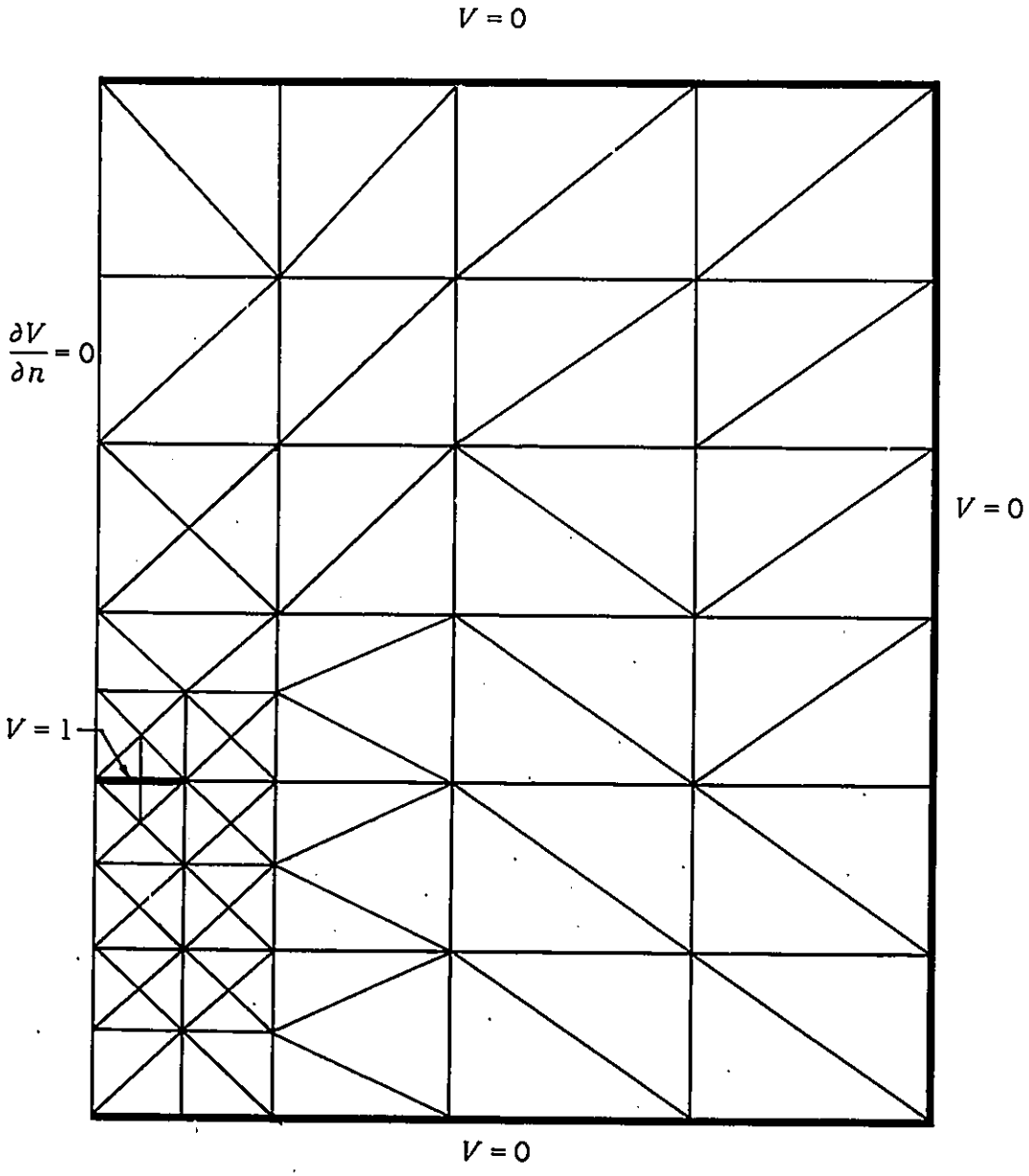

Fig.6

One half of the microstrip and its triangular Finite Element representation.

The calculations to determine the energy stored in the the fields and thus the capacitance were performed several times with an increasing number of triangles to improve the accuracy for each calculation. Linear regression was then used to extrapolate to large numbers of triangles where the results should converge. The calculated results using the Finite Element approach , along with the analytical results from appendix II are presented in the table below:

No. of triangles	Co (pF)	C (pF)	Zo (ohms)
27	34.4	109.2	54.4
42	27.8	48.0	68.8
79	26.2	78.7	73.4
analytical	--	--	86.3

Table I
Calculated values of the Characteristic Impedance

The results in Table I along with the linear approximation

$$(y = -7.84x + 84.7) \tag{50}$$

of the results are plotted in Figure 7. From the linear regression results the characteristic impedance is found to be converging to 84.7 ohms.

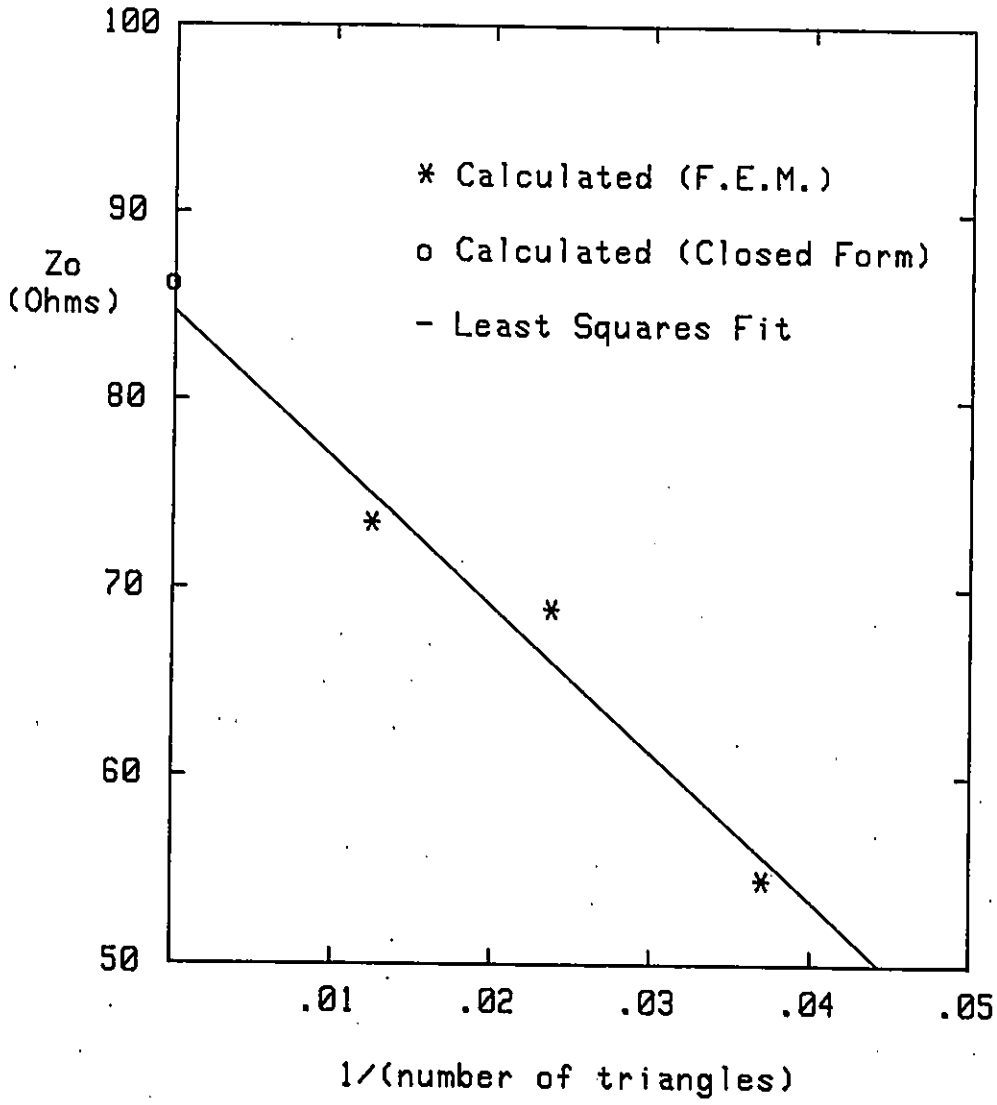

Fig. 7

Calculated Values of Characteristic Impedance

3.3 Multiple Images

Since there is an air/dielectric boundary at x = h, reflections from this boundary must also be considered. microstrip transmission lines theoretically have an infinite number of images above the dielectric and below the ground plane with the separation distance dependent upon the location of the line with respect to the air/dielectric boundary [15]. Figure 8 presents the multiple images for the case where the line is located at the air/dielectric boundary.

Assuming the current distribution resembles the charge distribution presented in the static case [15], the resulting field will then be a superposition of the fields due to each image as well as the line. To calculate the effect of the multiple images the magnetic vector potential for each image could be calculated and the vector sum taken to produce the net field. The geometry, and in particular, expressing the distance from each image to the point of interest would be very tedious. Alternatively one could consider the images as an N element array of sources equally spaced and with non-uniform amplitudes. The array factor A_f could then be calculated and the resulting field expressed as:

$$E_{total} = E_{singleelement} \times A_f \qquad (51)$$

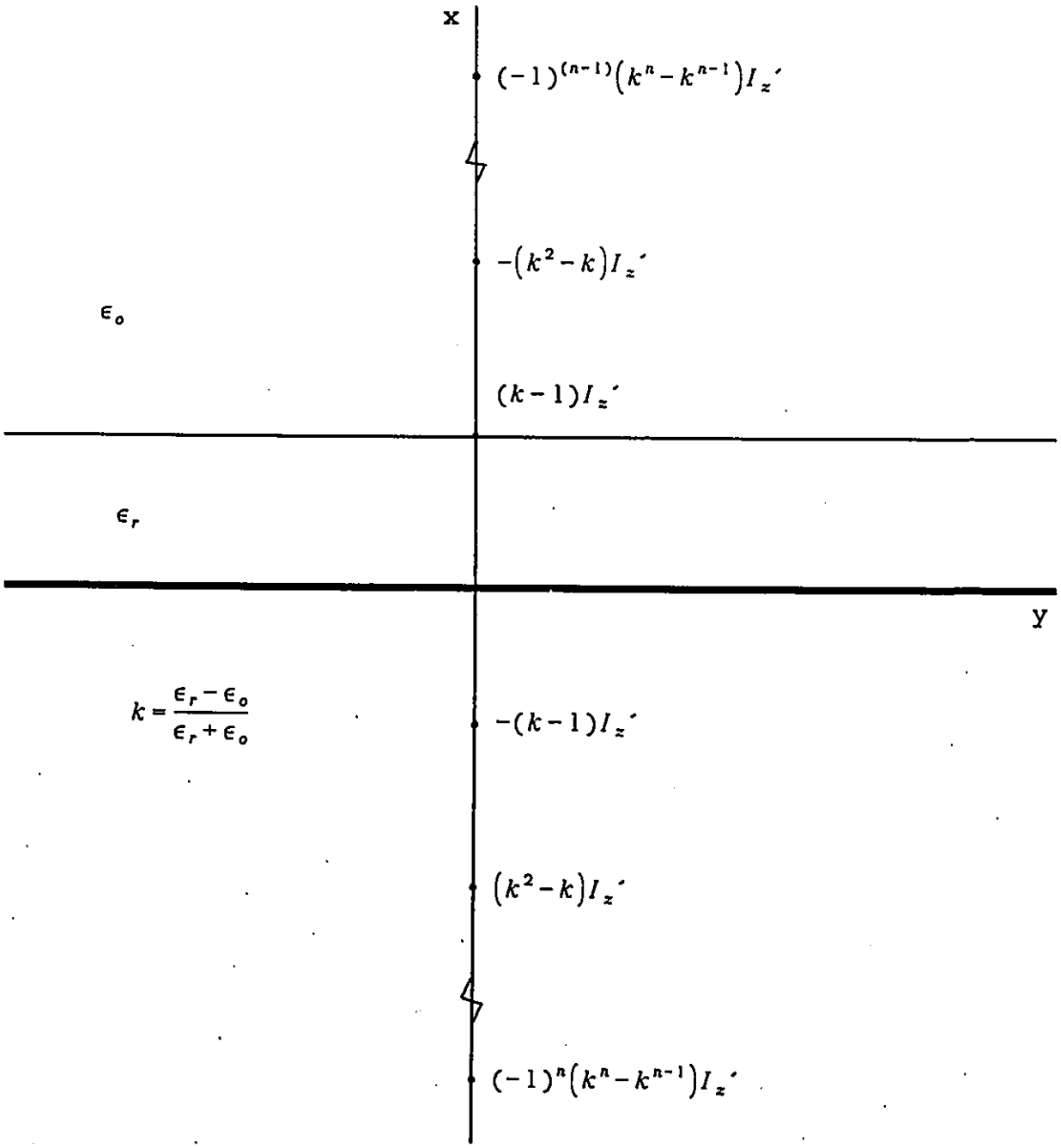

Fig. 8

Arrangement of multiple images due to air/dielectric boundary

The array factor (Af) for 2M uniformly spaced sources on the x axis [5] is given by:

$$Af = \sum_{n=1}^{M} A_n \cos\left\{\frac{2n-1}{2}(kd\cos\gamma + \beta)\right\} \qquad (52)$$

Where:

A_n = element amplitude

$k = 2\pi\lambda$

β = Phase variation between elements

d = separation between elements

$\gamma = \cos^{-1}(\sin\theta\cos\phi)$ = angle between the array axis and the point of observation

For small h ($h << \lambda$) the array factor should not significantly affect the radiation pattern.

Calculations of the array factor are performed neglecting all images except for the main (first) image below the ground plane to reflect the situation without the dielectric present. The array factor will then be calculated for multiple images to show the potential effect of the dielectric on the radiation pattern.

The calculations for the array factor (Af) for M=2 (a single image below the ground plane and no images due to the air/dielectric boundary) and M=12 (11 images plus the conductor) are presented in Table II below. Due to the symmetry involved the array factor is calculated for only one quadrant. The complete pattern is a "figure 8" with maximums at $\phi = 0°, 180°$ and nulls at $\phi = 90°, 270°$.

ϕ	$Af(dB)$ 1 image	$Af(dB)$ 12 images
0	0.0	0.0
10	-.133	-.133
20	-.541	-.540
30	-1.25	-1.25
40	-2.32	-2.31
50	-3.84	-3.84
60	-6.03	-6.02
70	-9.33	-9.32
80	-15.2	-15.2
90	-200	-200

Table II

Array factor vs angle off axis (γ)

Referring to Table II it is clear that for this application multiple images have no significant impact on the radiated fields and the dielectric in the microstrip can be ignored once the characteristic impedance is determined.

3.4 Electric Field Calculations

3.4.1 Method I

To calculate the fields using method I (magnetic vector potential) equation (5) from Section 2.1 must first be solved. Recalling from Equation (5):

$$A = \frac{\mu}{4\pi}\int_0^l I_o(z')\frac{e^{-jkR}}{R}dz' \tag{53}$$

The current distribution $I_o(z')$ along the line is calculated using classical transmission line theory [2,10] and is:

$$I(z') = \frac{V_o Z_c}{Z_c(Z_o + Z_l)\cos kz' + j(Z_c^2 + Z_o Z_l)\sin kz'} \tag{54}$$

Referring to Figure 2, the distance from any point along the line to the point of interest is expressed as:

$$R = \sqrt{(x-x')^2 + (y-y')^2 + (z-z')^2} \tag{55}$$

Converting to spherical coordinates:

$$x' = r\sin\theta\cos\phi$$

$$z' = r\cos\theta$$

$$y' = 0$$

Equation (55) can be re-written as:

$$R = \sqrt{x^2 + y^2 + z^2 + \left(-2r\sin\theta\cos\phi x' + x'^2\right) + \left(-2r\cos\theta z' + z'^2\right)} \qquad (56)$$

Substituting $R_o^2 = x^2 + y^2 + z^2$, expanding in a binomial series and taking the first two terms the following expression for the distance from any point on the line above ground to the point P of interest is obtained:

$$R = R_o - z'\cos\theta - \frac{b}{2}\sin\theta\cos\phi \qquad (57)$$

A similar expression can be found for the distance from any point on the image to point P:

$$R = R_o - z'\cos\theta + \frac{b}{2}\sin\theta\cos\phi \qquad (58)$$

Substituting equations (54, 57 & 58) into (53) the solution for the magnetic vector potential is now given [2]:

$$A_x = \frac{V_o \mu b}{4\pi D}\frac{e^{-jkr}}{r}\left(Z_o e^{jkl\cos\theta} - Z_o\cos kl - jZ_s\sin kl\right) \qquad (59)$$

and

$$A_z = \frac{V_o \mu b\cos\phi e^{-jkr}}{4\pi D\sin\theta r}B \qquad (60)$$

where:

$$B = Z_o\left(\cos\theta e^{jkl\cos\theta} - \cos\theta\cos kl - j\sin kl\right) + Z_s\left(e^{jkl\cos\theta} - j\cos\theta\sin kl - \cos kl\right) \qquad (61)$$

and

$$D = Z_o(Z + Z_s)\cos kl + j(Z_o^2 + ZZ_s)\sin kl \tag{62}$$

Rectangular to spherical conversion [5] can be used to provide the magnetic vector potential in terms of ϕ and θ as follows:

$$A_\theta = A_x \cos\theta\cos\phi - A_z \sin\theta \tag{63}$$

$$A_\phi = -A_x \sin\theta \tag{64}$$

$$A_r = 0 \tag{65}$$

The magnetic vector potential can now be used to calculate the electric field using equation (6):

$$\bar{E} = -j\omega\bar{A} \tag{66}$$

By replacing the ground plane of the microstripline with an image located below the plane the separation distance between the line and its image will now be twice the height of the microstripline. Taking this into account the source voltage as well as source, load and characteristic impedances will also be doubled.

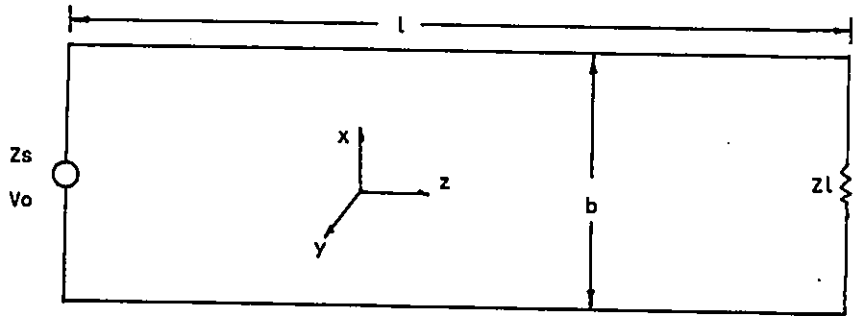

a) Model for Analytical Solution

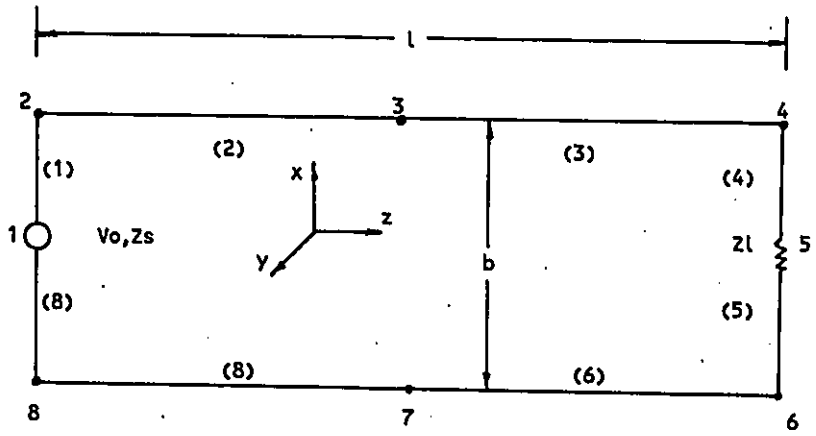

b) Wire Grid Model for M.O.M

Fig. 9

Transmission Line Orientation

The values used for the calculations (presented below) are based on practical values currently being used in industry.

Vo = 2.8 V.
Zs = 100 ohms
Zl = 172 ohms
Zo = 172 ohms
l = .252 m.
b = 2h = .32 cm.

The results for both E_θ and E_ϕ are symmetric about the $\phi = 0°, 90°$ axis in the $\theta = 90°$ plane. Results for one quadrant are presented in Table III.

	Field (dBuV/m)	
ϕ	$\lvert E_\theta \rvert$	$\lvert E_\phi \rvert$
0	60.8	-69.3
10	60.7	45.6
20	60.3	51.5
30	59.5	54.8
40	58.5	57.0
50	57.0	58.5
60	54.7	59.5
70	51.5	60.3
80	45.6	60.7
90	-59.6	60.8

Table III

Radiated fields in the $\theta = 90°$ plane

3.4.2 Method II

The approach used for method II (Method of Moments) is to replace the existing structure with a wire grid model where the wire grid represents the current flow.

As a first approximation the microstrip line is replaced with a single wire grid of equivalent cross sectional area and the ground plane is replaced with an image similar to that of method I. The length of each section for the wire grid should be less than $\lambda/16$ for suitable accuracy [16]. By choosing two segments to represent the length of the line this requirement is met and computing time should be minimal.

Again due to symmetry the results obtained by this method are presented in table IV below for one quadrant only.

	Field (dBuV/m)	
ϕ	$\lvert E_\theta \rvert$	$\lvert E_\phi \rvert$
0	61.6	-160
10	61.4	40.4
20	61.0	51.3
30	60.3	54.2
40	59.2	55.8
50	57.7	57.0
60	55.5	57.9
70	52.2	57.9
80	46.3	58.8
90	24.5	58.7

Table IV

Radiated fields in the $\theta = 90°$ plane

3.5 Test Site Calculations

As outlined previously, the objective is to calculate the electric field one would expect to measure at a test site used for FCC compliance measurements as opposed to the free space results presented in Section 3.4.

Figure 10 presents the test arrangement used for compliance measurements. To predict the fields for this situation, the influence of the test site ground plane must be considered. Since the microstripline radiates only into its upper hemisphere, only orientation II of Figure 10 (microstripline perpendicular to the ground plane) will require calculations for both the direct and reflected signal.

To perform the calculations the ground plane will be replaced with an image equivalent to the microstripline, i.e. equivalent magnitude and phase for vertical sources and equivalent magnitude and 180 degree phase shift for horizontal sources. The field at the receive antenna will be the vector sum of the fields produced by the two sources, taking into account the different path lengths. This can be expressed as:

$$E_{total} = 2E_s \cos(1/2kd\cos\theta + \beta) \qquad (66)$$

where: E_s is the free space microstripline field
d is the separation distance of the two sources
θ is the angle between the axis of the sources and the direction of radiation
$\beta = 0$ for vertical fields and π for horizontal fields.

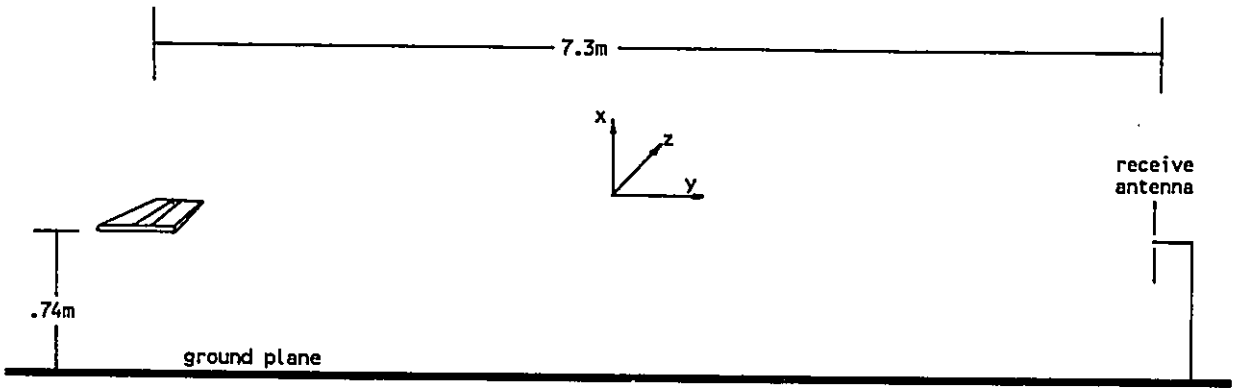

Orientation I

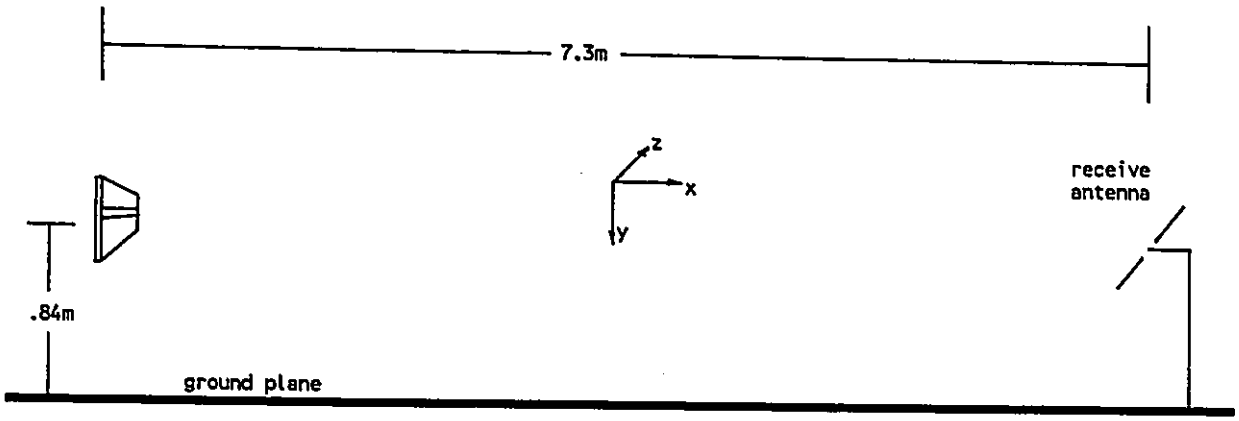

Orientation II

Fig. 10

Test Orientations

The effects of a mismatch on the transmission line are demonstrated by performing calculations for three situations; matched transmission line (Zl=86 ohms), high impedance termination (Zl=5000 ohms) and low impedance termination (Zl=5 ohms).

Although arbitrary, the values chosen are beyond the range of input impedances one would expect to find in digital logic devices. The intent here is to demonstrate the effects of termination impedance and predict worst case bounds that may be expected for a given design. The fields are calculated at a distance of 30 m. for comparison with the FCC Class A limits.

Figures 11 and 12 present the results for the E_x (orientation I, vertical polarization) and E_z (orientation II, horizontal polarization) cases.

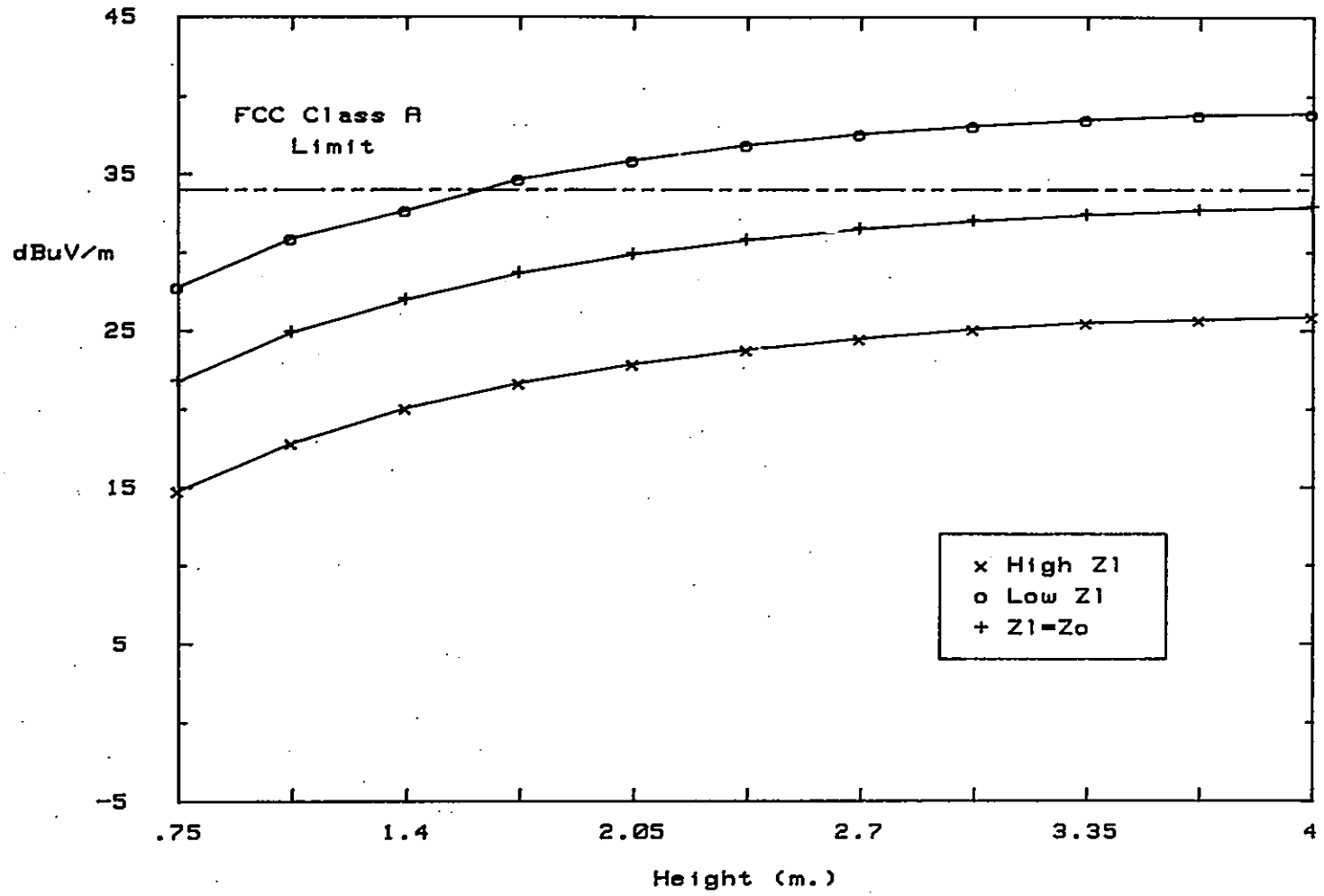

Fig. 11

E_z vs height for various termination impedances

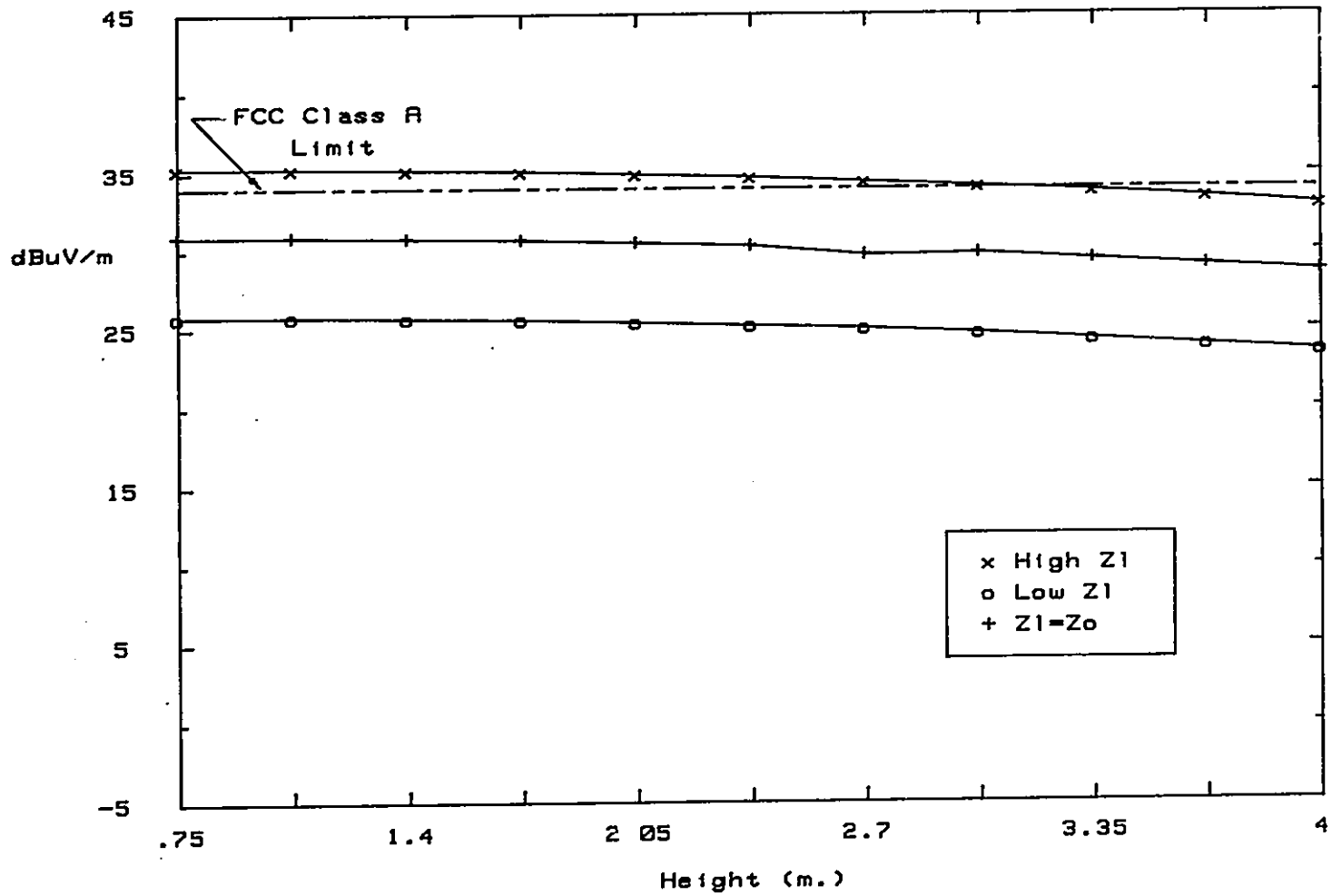

Fig. 12

E_x vs height for various termination impedances

3.6 Discussion of Calculated Results

The analysis presented here is based on two well known techniques for determining radiated fields from current carrying wires. To apply the techniques to a microstrip transmission line, the microstrip structure was replaced with a two wire transmission line and the radiation from that structure calculated.

From Tables III and IV it can be seen the differences between the two methods is +1.2 dB for $E_{\theta max}$ and -2.1 dB for $E_{\phi max}$ for the calculations performed in the $\theta = 90°$ plane. As the radiation pattern approaches a null the differences tend to increase. Both methods have associated strengths and weaknesses for this application and will be discussed individually.

A. Method I

Estimating the current distribution along the wire using transmission theory and then determining the magnetic vector potential and electric field requires very little programing to produce acceptable results.

Although the program used for the field calculations in this work was in Fortran, it could easily be converted to Basic for implementation on a personal computer, an attractive feature for this method considering the availability of these products.

The major weakness with this method is in applications of more complex geometries such as bends or branches in the microstrip. The current distributions and fields would have to be calculated for each branch and then summed to produce the resultant field. Although not difficult, the effort does increase with the complexity.

The results obtained for the characteristic impedance using a very simple closed form expression presented in Appendix II are sufficiently close to the Finite Element results that the added effort would not be necessary in most applications. The closed form expression could be included in the same program used to calculate the magnetic vector potential and electric field.

The characteristic impedance is also required during the design stage of the product and this calulation would also function as a design check.

B. Method II

The second technique, the Method of Moments requires significant computing capability to realize a useful tool although there are now many programs available and one would not have to be produced.

Since the structure to be studied is represented by a wire grid model, complex geometries can easily be realized and modified. For structures where the conductors are wide, a single wire would not be sufficient to model the conductor and each conductor should be represented by a grid. For this situation several iterations may have to be performed, modifying the segment lengths and node points to match the current distributions. As the grid structure becomes finer the solution should converge.

Effects of termination impedance.

The terminating impedance used on the transmission line is also shown to impact the levels of radiated emissions from the microstripline. Figures 11 and 12 present the results obtained using method I (Analytical) for the transmission line terminated in several different impedances.

From these plots it is seen that the dominant polarization is dependent upon the current distribution. For the high impedance situation, the horizontal component of the field is larger than the vertical component. The current distribution is primarily along the transmission line with little current appearing in the termination. As the terminating impedance is lowered, the vertical field component increases as the current in the termination increases.

Although some radiation can be expected from the termination, at the frequencies addressed in this work the termination is electrically quite small and will contribute very little to the total radiated field. Both methods used in this work take the termination into account. In the analytical case, the current distribution is assumed to be uniform. The M.O.M. procedure assumes a lumped resistance at the center of the termination. A sinusoidal current is then approximated across the termination although in this case the segment length in the termination is much smaller than a wavelength and the current distribution appears uniform.

The characteristic impedance for a microstrip is usually chosen based on other design objectives and can not easily be changed to suit EMC requirements. This work however, highlights the need for a properly terminated microstripline to provide control over the radiation from the line.

4 Experimental Measurements

4.1 Characteristic Impedance

To demonstrate that the Finite Element Method for determining the characteristic impedance of the microstrip is valid, the input impedance to the line was measured using an HP 8753A Network Analyzer. The transmission line was terminated in 86 ohms, the characteristic impedance calculated in Section 3.2 and the forward reflection coeffiecient measured. Figure 13 presents the Smith chart plot of the S_{11} measurement (forward reflection coefficient).

The measurement is normalized to 50 ohms (the impedance of the network analyzer) thus the center of the plot represents 50 ohms. Although the plot indicates the input impedance of the microstripline is not matched to the analyzer (i.e. not 50 ohms), it does show the input impedance is reasonably constant over the frequency range (50 - 250 MHz) indicating a close match between the microstripline characteristic impedance and the termination resistance. A perfect match would be presented here as a single input impedance over the frequency range.

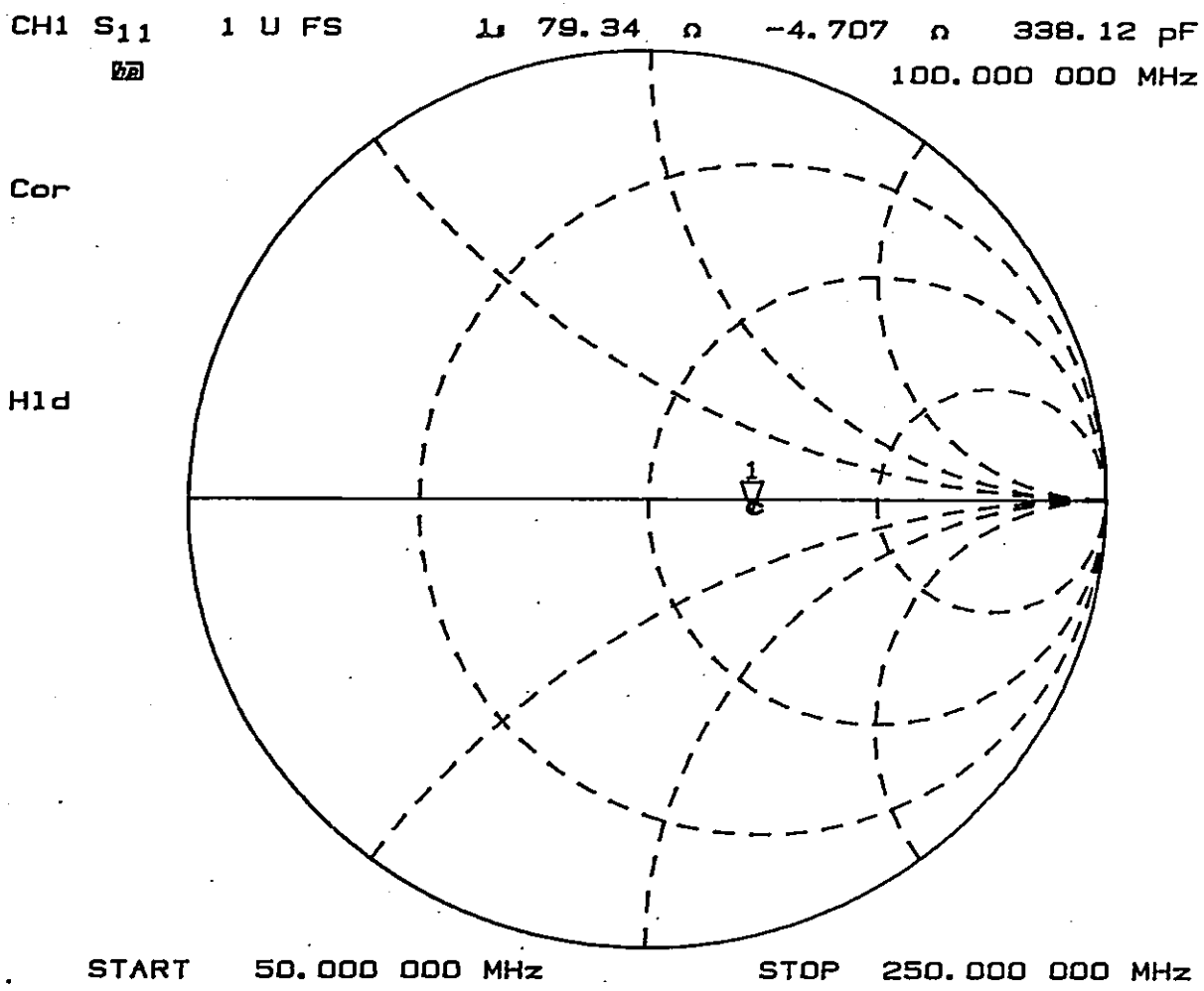

Fig. 13

Input impedance for the microstrip terminated in 86 ohms

4.2 Radiated fields

The general approach here is not to characterize the microstrip as an antenna but rather to establish its radiation relative to the FCC requirements. As such the radiation from the microstrip will be measured using the FCC test methods as opposed to determining the radiation pattern in a free space environment.

4.2.1 Measurement setup

Measurements of the radiated fields were made using an FCC type 'Open Field' test site normally used for compliance verification measurements. The site consists of a fiberglass building erected on a 10m X 20m ground plane. The dimensions and test configuration are detailed in Figure 10 and Figure 14. The FCC open field test site varies from a traditional antenna test range in that the equipment under test (EUT) is generally located close to ground (1m. above ground). The receiving antenna height is adjusted over a height range of 1-4 m searching for maximum received signal thereby measuring the sum of the direct plus ground reflected waves from the the EUT. Location of the antenna is usually 3m from the EUT for small products (1 m square) and 10m for larger equipment. In contrast antenna measurements are generally measured in free space (no ground influence) unless specific intormation is required about the behavior of the antenna near ground.

The consideration in selecting a test configuration was to be in the far field to ensure a plane wave. Unfortunately as the distance from the microstrip increases, the angle subtended between the microstrip and the receiving antenna when the antenna is at maximum height (4 m) decreases, limiting the range of angles to compare with the calculations.

The far field transition can be determined from:

$$2D^2/\lambda \tag{68}$$

where D is the maximum dimension of the radiating structure or receiving antenna.

For a test frequency of 100 MHz, $D = \lambda/2 = 1.5m$ and the transition to far field occurs at 1.5m thus a 3m measurement could be made. The preferred distance to ensure a plane wave field would be at least 10m but to maximize the change in angle and contend with test site availability, a separation distance of 7.3m was eventually used for the measurements.

Printed circuit board mounting in electronic products usually takes one of two forms. Single board products usually have the PCB mounted horizontally in the base whereas products with multiple boards usually have the boards mounted vertically in a card cage arrangement.

To represent both situations, measurements are made both with the microstrip parallel and perpendicular to the ground plane.

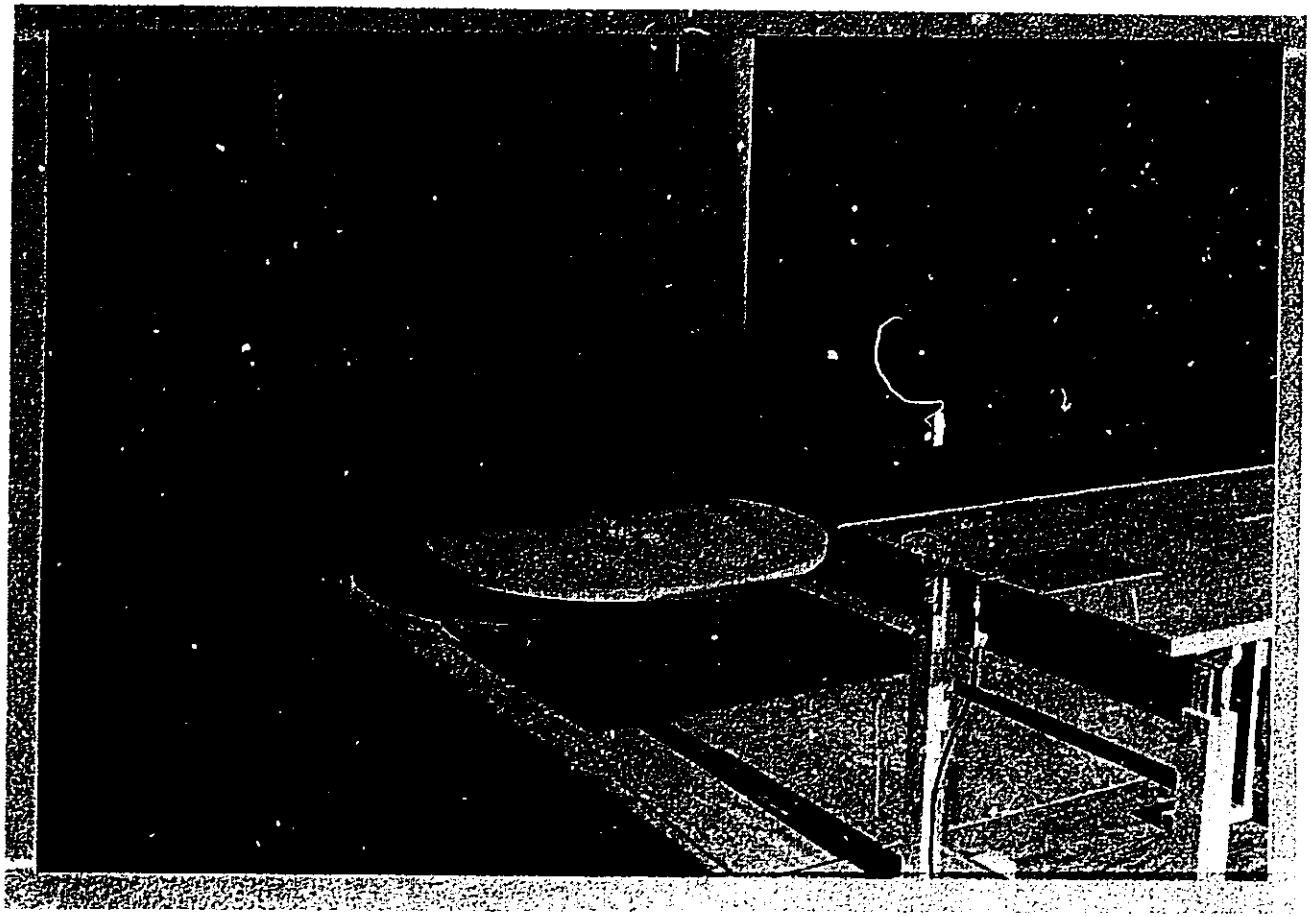

Fig. 14

Test configuration

4.3 Test method

To measure the radiated fields from the microstrip, a dipole tuned to 100 MHz and spectrum analyzer were used. The spectrum analyzer was set to sweep at the same rate the antenna positioner traversed the .75 to 4.0 m height. In this way the field could be recorded continuously and any abnormalities (narrow peaks or nulls) detected.

The settings for the spectrum analyzer were as follows:

Center frequency....100 MHz
Frequency span.....0 Hz
Sweep rate.....30 sec.
Max. hold
Single sweep

The antenna positioner and spectrum analyzer sweep could now be activated simultaneously and the resulting x axis of the analyzer display would be proportional to height above ground (or θ)

4.4 Test Results

To convert the antenna output voltage (Vr) measured by the spectrum analyzer to field strength, the received voltage must be corrected as follows:

$$E(dB\mu V/m) = V(dB\mu V) + A_F(dB) + C_L(dB) \qquad (69)$$

where:

$E(dB\mu V/m)$ is the field strength
$V(dB\mu V)$ is the received voltage
A_F is the antenna correction factor
C_L is the cable loss

For direct comparison with the FCC Class A limits the field measured at 7.3 m. was extrapolated to the 30 m. distance. For far field conditions the field intensity is inversely proportional to the distance from the source (66) and a -12.3 dB ($20\log(7.3/30)$) correction factor is used.

Using $A_F = 10dB$ and $C_L = 5dB$ the spectrum analyzer was offset to provide a display output in field strength directly.

Measurements were made per FCC rules i.e. vertical and horizontal orientation of the receive antenna with the antenna scanned to cover a height of 1-4m. Figure 15 and 16 present the maximum horizontal (E_x) and vertical (E_z) fields produced by the orientations in Figure 10.

Presented along with the measurements are the calculated results using the methods of Section 3.4.

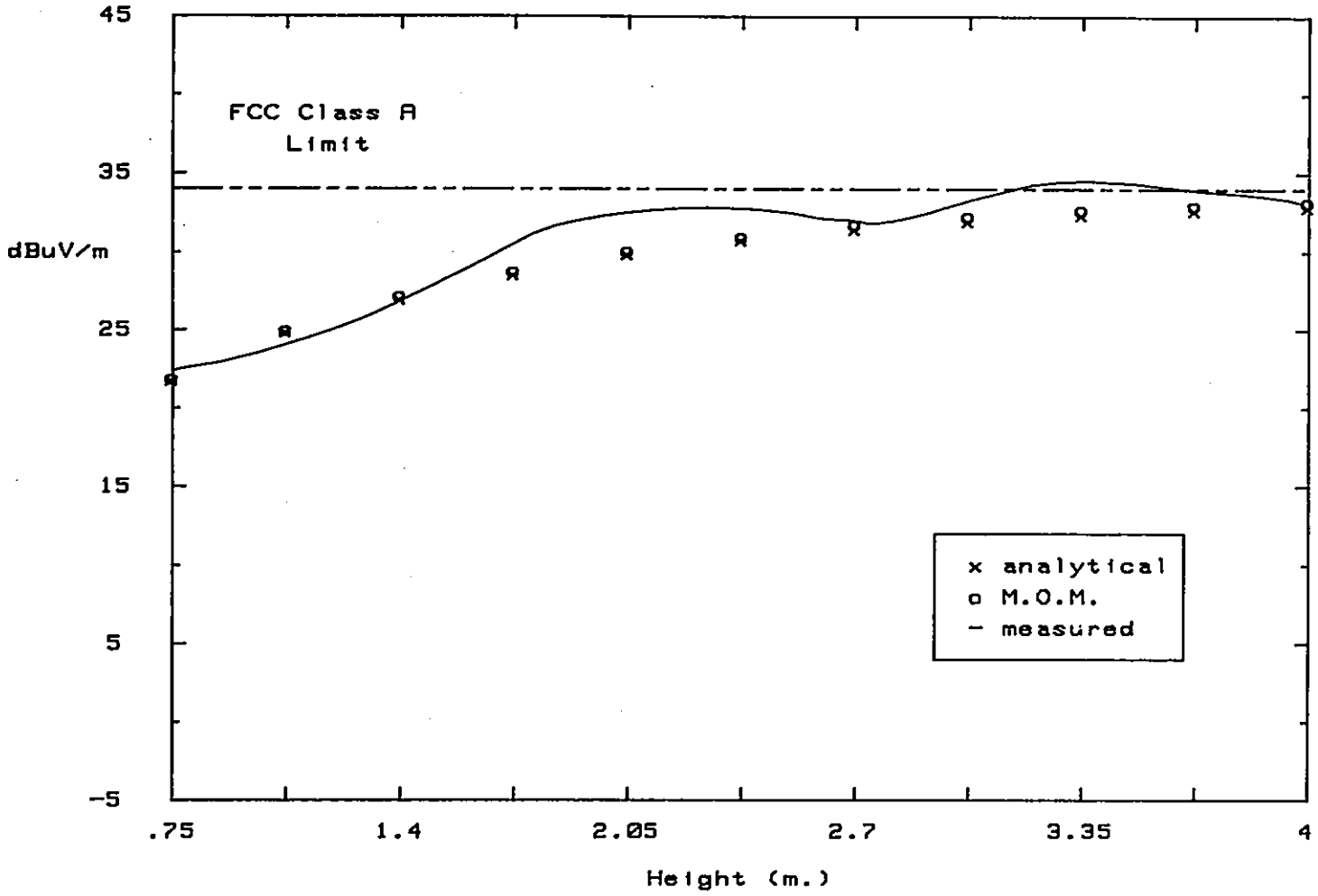

Fig. 15

E_z vs height above ground - orientation I

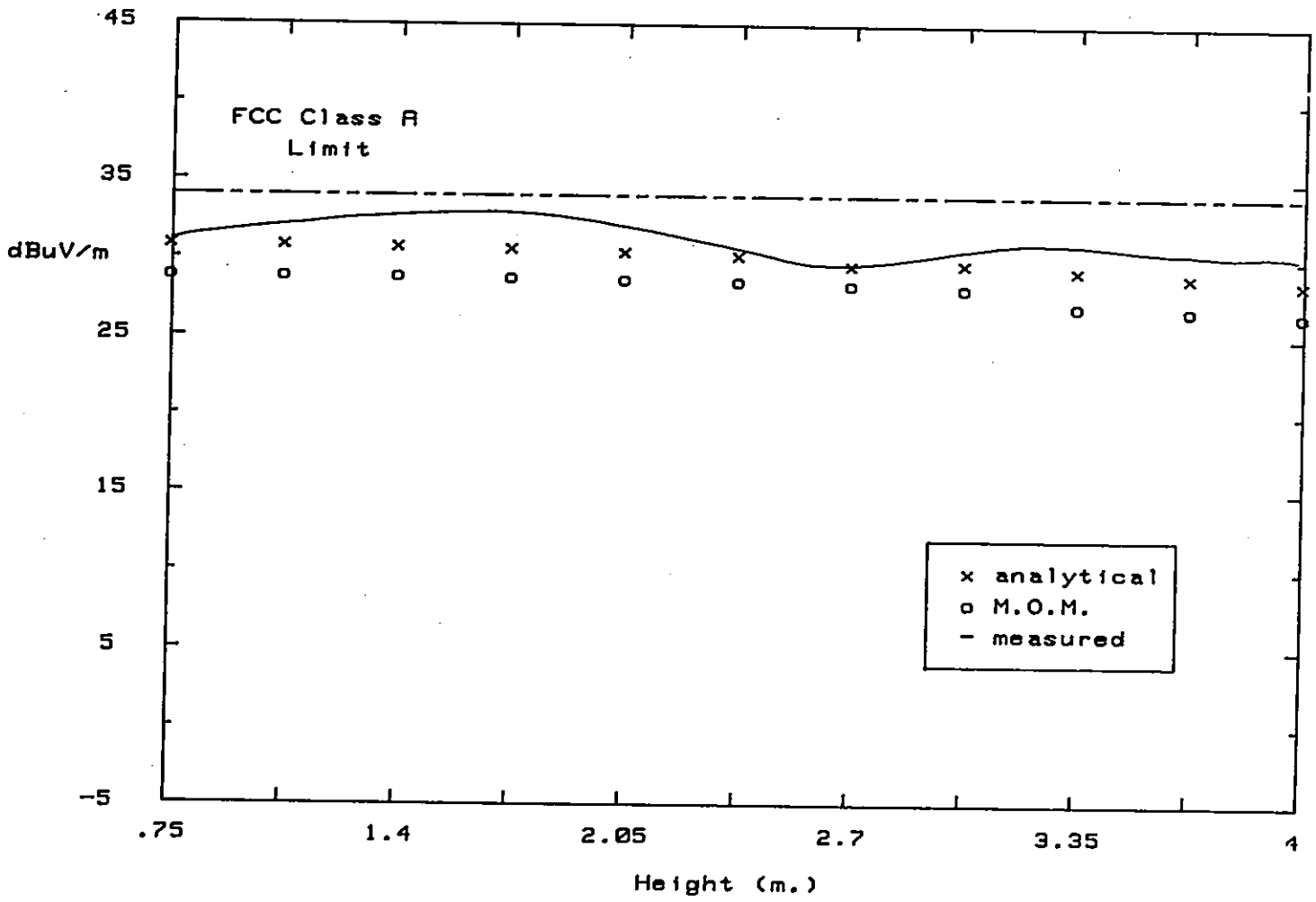

Fig. 16

E_x vs height above ground - orientation I

5 Conclusions

The calculations and measurements performed in this work are to demonstrate a method suitable for predicting electric field radiation from printed circuit boards. By accurately establishing the levels of radiation from such a board during the design stage, valuable time can be saved and costly redesign may be avoided. If analysis is not performed at the design stage, problems with high levels of radiation may not be apparent until the FCC compliance test is performed on a prototype, or even production unit, depending on the time constraints. Should that happen, modifications may be costly and drastically change the product appearance (i.e. heavy shielding and filtering), resulting in reduced profits and potentially an undesirable product.

Tables III and IV indicate that for printed circuit boards parallel to the ground ($\phi = 90°$) , vertical electric fields predominate, whereas boards mounted vertically ($\phi = 0°$) would produce electric fields parallel to the circuit board traces. Also, since the microstrip radiates only into the hemisphere above the board, reflections from the ground plane at the test site are only significant for vertically mounted printed circuit boards of microstrip design.

Circuit boards without ground planes would radiate into both hemispheres and the analysis should be modified accordingly.

As can be seen from Figure 15 and 16 the predictions closely match with the measurements in the case of both the vertical and horizontal mounted printed circuit boards.

Clearly performing calculations to determine compliance of a product with the FCC regulations one must take into account the test geometry used and the resulting field strength calculated taking both the direct and reflected fields into account. Without considering the reflected field the calculations would be 6 dB

low at angles where both fields are in phase. The magnitude of the error will depend on the frequency of the emission being measured. At low frequencies the two fields will not be completely in phase over the 1-4 m search height and the calculations would predict on the low side. As the frequency increases there may be several nulls and peaks over the 1-4 m height.

Predicting the radiation from a circuit using digital techniques would require determining the harmonic content of the signals prior to applying the techniques presented here. By using the Fourier Transform the amplitudes of the signal harmonics could be obtained and the calculations made to determine the radiated fields at the various frequencies.

Steps to reduce the levels of radiation could be taken in a number of ways. Referring to equations (59) and (60) it is seen that the fields are proportional to the signal drive levels and the microstrip thickness. By waveshaping to reduce harmonic content, lowering signal drive levels and reducing the dielectric thickness between the conductor and ground, the EMC characteristics of a design could be improved.

The techniques presented here have previously been investigated [17] to determine the currents induced in a transmission line illuminated by an incident electric field. The objective there is to reduce the susceptibility of a circuit to Electromagnetic Interference. As demonstrated in this work, the electric field emissions from a microstrip transmission line can also be predicted with a high degree of accuracy by simplifying the problem to a two wire structure and ignoring the effects of the dielectric (once the microstrip characteristic impedance has been determined).

6 Appendix

I. Magnetic Vector Potential

In electromagnetic studies, the magnetic vector potential ($\bar{A}$) is a useful tool in determining the electric and magnetic fields resulting from current and magnetic sources.
$\bar{A}$ will be developed here for applications in Section 2.

Starting with Maxwell's equations:

$$\nabla \times \bar{E} = -j\omega \bar{B} \tag{70}$$

$$\nabla \cdot \bar{E} = \rho / \epsilon_0 \tag{71}$$

$$\nabla \times \bar{H} = j\omega \epsilon \bar{E} + \bar{J} \tag{72}$$

$$\nabla \cdot \bar{H} = 0 \tag{73}$$

Since the divergence of H is zero, it can be represented by the curl of some other vector using the vector identity:

$$\nabla \cdot (\nabla \times \bar{A}) = 0 \tag{74}$$

We can now write the magnetic field H as:

$$\bar{B} = \mu \bar{H} = \nabla \times \bar{A} \tag{75}$$

where $\bar{A}$ is the magnetic vector potential. Although not a physical entity, $\bar{A}$ will be useful in determining the electric field E.

Substituting (75) into (70) and re-arranging results in:

$$\nabla \times [\bar{E} + j\omega \bar{A}] = 0 \tag{76}$$

From the vector identity:

$$\nabla \times (-\nabla \phi) = 0 \tag{77}$$

where ϕ is a scalar, the expression in the brackets of equation (73) can now be equated to the gradient of a scalar.

$$\bar{E} = -j\omega \bar{A} - \nabla \phi \tag{78}$$

where ϕ is an arbitrary scalar electric potential.

Using the Lorentz condition:

$$\nabla \cdot \bar{A} = -j\omega \epsilon \mu \phi \tag{79}$$

the electric potential can be expressed in terms of the magnetic vector potential.

Substituting the expression for the electric potential from (79) back into equation (77), the electric field can now be written as:

$$\bar{E} = -j\omega \bar{A} - \frac{j}{\omega \epsilon \mu} \nabla (\nabla \cdot \bar{A}) \tag{80}$$

The electric field can be determined once an expression for $\overline{A}$, the magnetic vector potential is found. Returning to equation (75) and taking the curl of both sides:

$$\nabla \times (\mu \overline{H}) = \nabla \times \nabla \times \overline{A} \tag{81}$$

Using the vector identity:

$$\nabla \times \nabla \times \overline{A} = \nabla(\nabla \cdot \overline{A}) - \nabla^2 \overline{A} \tag{82}$$

Equation (81) can now be expressed in terms of the magnetic vector potential:

$$\mu \nabla \times \overline{H} = \nabla(\nabla \cdot \overline{A}) - \nabla^2 \overline{A} \tag{83}$$

Substituting equation (72) into equation (83) we obtain:

$$\nabla^2 \overline{A} = \nabla(\nabla \cdot \overline{A}) - j\omega\mu\epsilon\overline{E} - \mu\overline{J} \tag{84}$$

The expression for the electric field given by equation (79) can now be used in (84) to give:

$$\nabla^2 \overline{A} = -j\omega^2\epsilon\mu\overline{A} - \mu\overline{J} \tag{85}$$

Re-arranging equation (85) provides the general form of the Wave Equation:

$$\nabla^2 \overline{A} + k^2 \overline{A} = -\mu\overline{J} \tag{86}$$

where $k^2 = j\omega^2\epsilon\mu$

The general solution to equation (86) is [5]:

$$\bar{A} = \frac{\mu}{4\pi} \int_{v'} \int \int J \frac{e^{-jkR}}{R} dv' \tag{87}$$

The solution of the electric field can now be obtained in a two step procedure. First the magnetic vector potential, $\bar{A}$, can be found using (87) and the result used in equation (80) to obtain the electric field. Alternatively, equations (80) and (87) can be used to derive Pocklington's integral equation. Although not solvable analytically in most cases, this expression can be solved using a numerical technique such as the Method of Moments.

II. Characteristic Impedance

The characteristic impedance of a microstrip can be determined analytically using conformal mapping techniques [8]. In addition, numerous workers [7,8,9] have developed expressions based on empirical results.
The following expression given by Schneider [9] was selected for its simplicity and is included here for comparison.

The characteristic impedance of a microstrip with dielectric thickness h and conductor width w is given by:

$$Z_1 = \frac{60}{\sqrt{\epsilon_{e//}}} \ln\left(\frac{8h}{w} + \frac{w}{4h}\right) \tag{88}$$

The effective dielectric constant $\epsilon_{e//}$ is expressed by:

$$\epsilon_{e//} = 1 + q(\epsilon_r - 1) \tag{89}$$

where the filling factor is determined from:

$$q = \frac{1}{2}\left(1 + \frac{1}{\sqrt{1 + 10h/w}}\right) \tag{90}$$

Calculations using the dimensions outlined in Figure 4 result in a characteristic impedance of 86.3 ohms.

7 References

1. FCC Part 15j Rules and Regulations, 1980
2. C.W. Harrison and C.D. Taylor: "Response of a Terminated Transmission Line Excited by a Plane Wave Field for Arbitrary Angles of Incidence", IEEE Transactions on Electromagnetic Compatibility, Volume EMC-15, No. 3, August 1973
3. Y. Kami and R. Sato: " Radiation Model of Finite Length Transmission Lines", IEEE Electromagnetic Symposium, 1986
4. M. Costa, T.K. Sarkar, B.J. Strait and S. Bennett: "On Radiation from Printed Circuit Boards", IEEE international Symposium on Electromagnetic Compatibility, 1981
5. C.A. Balanis, "Antenna Theory, Analysis and Design", Harper and Row, 1982
6. R.P. Sylvester and R.L. Ferrare, "Finite Elements for Electrical Engineers", Cambridge University Press, 1983
7. T.C. Edwards, "Foundations of Microstrip Circuit Design", John Wiley and Sons, 1983
8. L.W. Cahill, "Approximate Formula for Microstrip Transmission Lines", Proceedings of the IREE, October 1974
9. M.V. Schneider, "Microstrip Lines for Microwave Integrated Circuits", Bell System Technical Journal, Vol. 48, No. 5, June 1969
10. A. Shadowitz, "The Electromagnetic Field", McGraw Hill, 1975
11. R.F. Harrington, "Field Computation by Moment Methods", R.E. Krieger Publishing Co., 1968
12. Stutzman and Thiele, "Antenna Theory and Design", John Wily and Sons Inc., 1981

13. J.H. Richmond, "Radiation and Scattering by Thin-Wire Structures in the Complex Frequency Domain", NASA Contract Report CR-2396, May 1974

14. J.H. Richmond, "Computer Program for Thin-Wire Structures in a Homogeneous Conducting Medium", NASA Contract Report CR-2399, June 1974

15. Y.M. Hill, N.O. Reckord and D.R. Winner, "A General Method for Obtaining Impedance and Coupling Characteristics of Practical Microstrip and Triplate Transmission Line Configurations", IBM Journal, May 1969

16. P.K. Agrawal and M.C. Bailey, "An Analysis Technique for Microstrip Antennas", IEEE Transactions on Antennas and Propagation, Volume AP-25, No. 6, November 1977

17. R.T. Abraham and C.R. Paul, "Coupling of Electromagnetic Fields onto Transmission Lines: A Comparison of the Transmission Line Model and the Method of Moments", RADC-TR--82-286, Vol. IV A, Rome Air Development Center, November 1982